Climatic cycles as expressed in sediments of the PROMESS1 borehole PRAD1-2, central Adriatic, for the last 370 ka: 2. Paleoenvironmental evolution

Andrea Piva

ISMAR, Consiglio Nazionale delle Ricerche, Via Gobetti 101, I–40129 Bologna, Italy (andrea.piva@bo.ismar.cnr.it)

Alessandra Asioli

IGG, Consiglio Nazionale delle Ricerche, Via Giotto 1, I–35100 Padova, Italy

Nils Andersen

Leibniz Laboratory for Radiometric Dating and Stable Isotope Research, CAU Kiel, Max-Eyth-Str. 11, D–24118 Kiel, Germany

Joan O. Grimalt

Department of Environmental Chemistry, Institute of Chemical and Environmental Research (IIQAB-CSIC), Jordi Girona 18, E–08034 Barcelona, Catalonia, Spain

Ralph R. Schneider

Institut für Geowissenschaften, Christian-Albrechts-Universität zu Kiel, Ludewig-Meyn-Str. 10, D–24118 Kiel, Germany

Fabio Trincardi

ISMAR, Consiglio Nazionale delle Ricerche, Via Gobetti 101, I–40129 Bologna, Italy

[1] The multidisciplinary study of planktic and benthic foraminifera, alkenone SST, and O and C stable isotope records allowed reconstruction of the paleoenvironmental history of the central Adriatic basin over the last 360 ka B.P. In general, the main paleoclimatic changes documented in the central Adriatic appear in phase with climate change in the North Atlantic realm, except for intervals which correspond to the deposition of sapropel levels in the eastern Mediterranean. In particular, the interval between Marine Isotope Stage (MIS) 7.5 and MIS 5 appears to be strongly influenced by the monsoonal regime. The comparison with other Mediterranean records also suggests that the Adriatic Basin was affected by very low sea surface temperature (SST) (down to 2°C for MIS 2) during glacial intervals, which is uncommon for the Mediterranean Basin. In addition, the SST record indicates that this basin was unable to maintain warm interglacial/interstadial conditions for durations similar to the western Mediterranean. This fact can be explained by the landlocked position and shallow depth of this basin, which make it particularly exposed to atmospheric forcing (e.g., Siberian High) and to the strong influence of the nearby landmass during glacial intervals, producing a lag in the demise of glacial intervals. Moreover, the progressively higher values of the $\delta^{18}O$ records of glacial intervals, alongside the SST record and the foraminifera assemblage, imply an increasing impact of the formation of cold and dense water since the penultimate glacial.

————————————

Theme: Interactions Between High-Frequency Climate Changes and Deltaic Margin Architecture
Guest Editors: S. Berné, J. Syvitski, and F. Trincardi

1. Introduction

[2] The Mediterranean Sea is a land-locked marginal basin, located between the high-latitude obliquity (41 ka)-driven climate system and the lower-latitude North African climate system, tightly linked to the precession cycle (21 ka). In this intermediate position, the Mediterranean Sea may have switched during the Quaternary between intervals more dominated by the former or by the latter climate system. To address the stability of the Mediterranean climate system high-resolution paleoceanographic studies can be based on records extracted from the broad shelves and upper slopes of the north central Adriatic and Gulf of Lyon, where very thick sedimentary sequences deposited during the last 500 ka. This interval encompasses several orders of cyclicity (100, 41, and 21 ka) that are characteristic of past Quaternary climate regimes. In addition, centennial to millennial-scale episodes of abrupt climatic change can be recognized as in Greenland and Antarctic ice cores records [*Dansgaard et al.*, 1993; *Petit et al.*, 1999; *EPICA Community Members*, 2004]. For these reasons, the central Adriatic and the Gulf of Lyon were selected by the European Community Profiles across Mediterranean Sedimentary Systems (EC-PROMESS 1) project to determine the stratigraphic response to glacio-eustatic sea level and climate change during the last 500 ka at Milankovitch and sub-Milankovitch (Dansgaard-Oeschger) scales.

[3] Borehole PRAD1-2 (Figure 1) is the first continuous and almost undisturbed marine record spanning the last 370 ka available from the Adriatic Basin [*Piva et al.*, 2008]. Consequently, bore-hole PRAD1-2 provides the first opportunity to analyze the paleoenvironmental changes of the last four glacial-interglacial cycles in the Adriatic, a key area for the oceanographic setting of the entire Mediterranean. Despite the shallow-water and proximal location where the borehole was drilled (186 m water depth), *Piva et al.* [2008] provided a multiproxy high-resolution integrated stratigraphy for PRAD1-2 (Figure 2), documenting a robust chronologic correlation with other oceanic records within and outside the Mediterranean, such as eastern Mediterranean sapropels and North Atlantic D-O events during Marine Isotope Stages (MIS) 3–5, respectively. This stratigraphic scheme is the base to investigate the climate linkages between the central Adriatic and Mediterranean/extra-Mediterranean areas (Figure 1). In addition, the Adriatic is a peculiar basin, whose morphology underwent significant and repeated changes in response to global sea level excursions driven by glacial-interglacial cycles. As an example, during the Last Glacial Maximum, circa 19–23 ka B.P., a large portion of the north Adriatic shelf was emerged, with the coastline located close to the −130 m isobath when the Po and the Apennine rivers discharged a huge amount of terrigenous material into the Basin [*Trincardi et al.*, 1994; *Cattaneo and Trincardi*, 1999].

[4] This paper aims at reconstructing the climatic trends of glacial and interglacial intervals during the last 370 ka in the central Adriatic. It integrates independent proxies, such as planktic and benthic foraminifera assemblages, foraminifera-derived O and C stable isotope composition, and alkenone-derived SST records. Comparison with other Mediterranean and extra-Mediterranean records provides information for the recognition of possible local
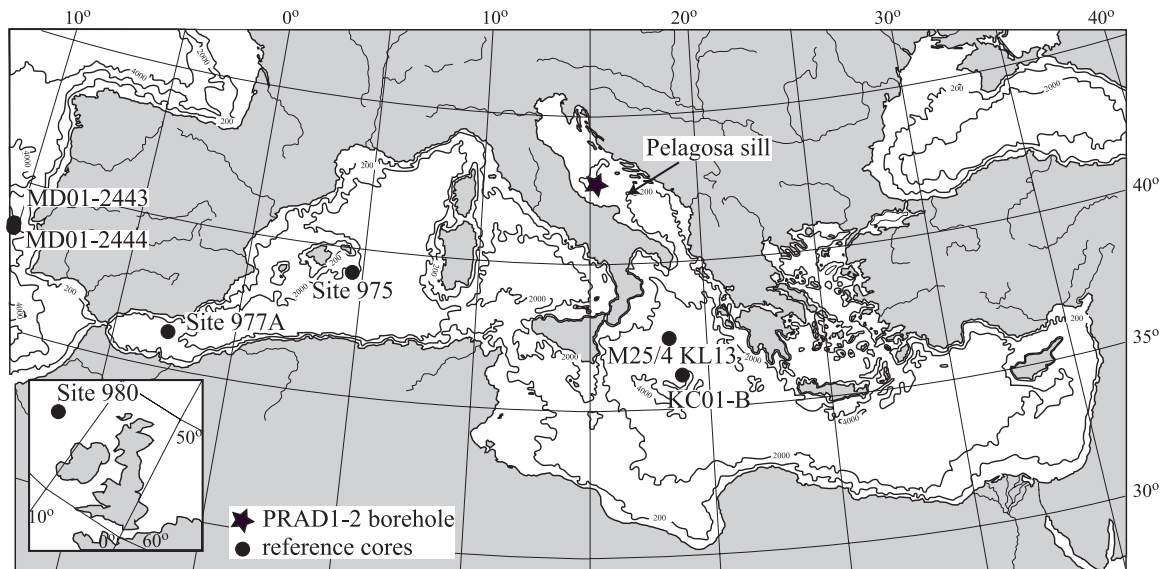
Figure 1. Location of borehole PRAD1-2 (star) and of core records (circles) discussed in the text.

effects, as well as the role this small basin played in the past for cold and dense water production.

2. Materials and Methods

[5] Borehole PRAD1-2 yielded a continuous, 71.2 m long sediment sequence, collected on the western slope of the Mid-Adriatic Deep, (LAT 42°40′34.7826″N, LONG 14°46′13.5565″E; 185.5 m water depth; Figure 1) by the geotechnical vessel BAVENIT, operated by FUGRO. The sedimentary record is formed by 89 core sections, each about 75–80 cm long and 6 cm in diameter. The borehole lithology, sketched in the log reported in Figure 2, is generally muddy with intervals of silty mud, while sand layers are present only in the lowest part of the hole, starting around 58 mbsf (section 73). Moreover, silty layers are typically the expression of volcanoclastic deposits reported in Figure 2, while it is noteworthy the presence of dark mud levels, illustrated by *Piva et al.* [2008] by means of pictures and color reflectance. After splitting, the working half of each core section was sampled for multiple analyses (micropaleontology and macropaleontology, sedimentology, magnetostratigraphy, isotope chemistry and sediment properties). The methods adopted for each proxy considered in the paper are summarized below; the reader is referred to *Piva et al.* [2008] for a complete description of all the other proxies taken into account in the integrated stratigraphy, such as magnetic properties (Anhysteretic Remanent Magnetization (ARM), inclination and declination), lightness, color reflectance, XRF data, radiocarbon ages.

2.1. Foraminifera

[6] In total, 784 subsamples were taken in 2 cm slices with a typical sampling interval of 10 cm. All subsamples were dried in the oven at 50°C, weighed, washed and sieved through a 63 μm mesh and dried again at 50°C. The samples were split into aliquots and a number of aliquots was counted to achieve a minimum of 300 planktic and 300 benthic specimens. The counting was performed on the fraction >106 μm, but the fraction <106 μm was always checked to avoid missing diagnostic species with elongated shell (such as *Fursenkoina*), or with small size in their adult stage (e.g., *Epistominella*). Some planktic species were lumped together according to the following scheme: *Globigerinoides sacculifer* included *Globigerinoides trilobus*, *Globigerinoides sacculifer* and *Globigerinoides quadrilobatus* (in the sense of *Hemleben et al.* [1989]), while warm species included *Globigerinoides* spp, *Orbulina* spp, *Zeaglobigerina rubescens* and *Globigerinella* spp. Planktic foraminifera that indicate high fertility of the surface water, such as Neogloboquadrinids, *Globigerina bulloides*, *Globigerinita glutinata* and *Globigerina quinqueloba*, have been lumped together and plotted in terms of flux (number of specimens per area unit per time unit) as a proxy of the surface plankton productivity. In the benthic assemblage, two proxies indicate different levels of bottom stress conditions: (1) the Oxygen
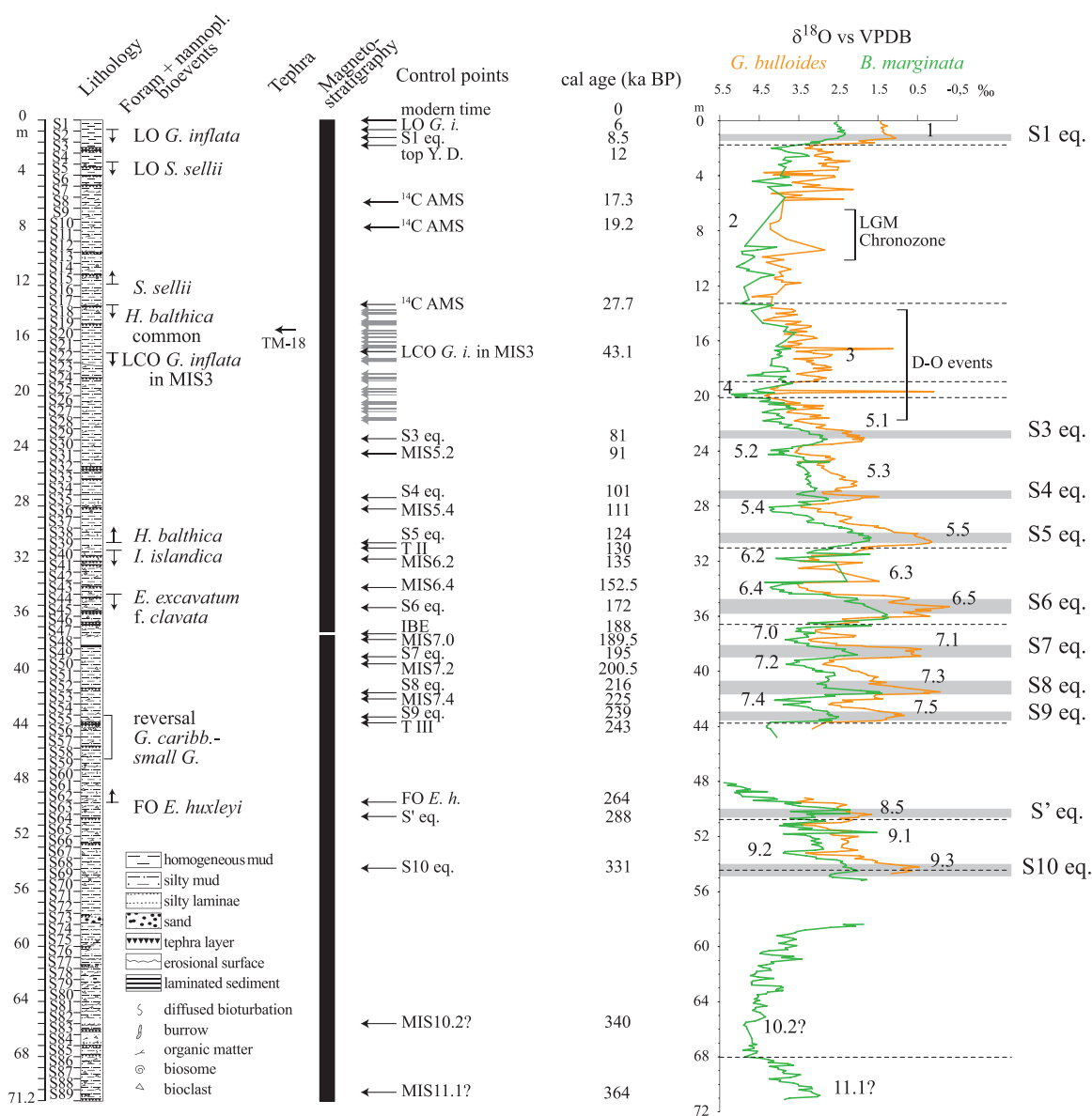
Figure 2. Stratigraphic framework of borehole PRAD1-2 [after *Piva et al.*, 2008]. From the left: core-section number, lithology, calcareous nannoplankton and foraminifera bioevents, position of the TM-18 tephra (Campanian Ignimbrite), control points (grey arrows denote Dansgaard-Oeschger events), chronology, and $\delta^{18}O$ records on planktic foraminifer *Globigerina bulloides* and benthic *Bulimina marginata*. Numbers refer to marine oxygen isotope stages (MIS) and substages; grey stripes mark the sapropel-equivalent layers. The ^{14}C AMS ages were calibrated using the online Calib 5.0.2 Radiocarbon Calibration Program [*Stuiver and Reimer*, 1993] for radiocarbon ages B.P. younger than 20,000 years and the online calibration program by *Fairbanks et al.* [2005] for ages older than 20,000 years.

Deficiency Stress (ODS) curve includes all those deep infaunal taxa particularly resistant to low-oxygen conditions, such as *Cassidulinoides*, *Fursenkoina*, *Glandulina*, *Globobulimina* and *Chilostomella* [e.g., *Rohling et al.*, 1997; *Jorissen*, 1999]; (2) the ''deep infaunal'' species curve includes taxa with infaunal microhabitat but less resistant to low-oxygen conditions, such as

Bolivina/Brizalina spp, *Uvigerina* spp, and *Bulimina inflata/costata* [e.g., *Jorissen*, 1999].

2.2. Oxygen and Carbon Stable Isotopes

[7] Stable oxygen and carbon isotope analyses were performed on selected monospecific specimens of foraminifera. On average, twenty specimens of *G. bulloides* (planktic) and *Bulimina*

marginata (benthic) were picked from the size fraction >180 μm for each analysis. The measurements were performed at the Leibniz Laboratory for Radiometric Dating and Stable Isotope Research, CAU Kiel, Germany, by the Kiel automated carbonate preparation device connected to a MAT 251 mass spectrometer. Each sample gas was measured ten times (in a reiterated succession of reference gas and sample gas). The external error of each measurement is better than 0.04‰ (δ^{13}C) and 0.06‰ (δ^{18}O). Isotope values are reported with respect to PDB standard.

2.3. Alkenones and Sea Surface Temperatures

[8] Subsamples (1 cm thick slices) were taken every 20 cm. The analytical procedure for determining the organic biomarkers is described in detail by *Villanueva et al.* [1997]. Briefly, samples were freeze-dried and manually grounded. After addition of an internal standard containing *n*-nonadecan-1-ol, *n*-hexatriacontane and *n*-tetracontane, ~2 g of dry sediment were extracted with dichloromethane in an ultrasonic bath. The extracts were saponified with 6% potassium hydroxide in methanol to eliminate interferences from wax esters. The neutral lipids were extracted with hexane which was then evaporated to dryness under a nitrogen stream. Finally, the extracts were redissolved with toluene, derivatized with bis(trimethylsilyl)trifluoroacetamide and analyzed by gas chromatography.

[9] The instrumental analysis of the samples was performed with a Varian gas chromatograph model 3400 equipped with a septum-programmable injector (Varian 8200CX) and a flame ionization detector. The carrier gas (hydrogen, 2.6 ml/min) passed through a CPSIL-5 CB column coated with 100% dimethylsiloxane (50 m long, 0.12 μm film thickness). The temperature program of the oven was as follows: the initial temperature 90°C was maintained 1 minute and then increased to 170°C at 20°C/min, then to 280°C at 6°C/min (holding time: 25 min) and, finally, to 315°C at 10°C/min (holding time: 12 min). The injector was programmed from 90°C (holding time 0.5 min) to 310°C at 200°C/min (holding time: 55 min). The detector was maintained with a constant temperature of 320°C.

[10] Selected samples were analyzed by gas chromatography coupled to mass spectrometry (GC-MS) for compound verification and identification of possible coelutions. GC-MS was performed with a Fisons MD800 (THERMO Instruments, Manchester, UK). The capillary column and the oven conditions were the same as described above. The carrier gas was helium at a flow of 2.1 mL/min. Injection port and transfer line temperatures were 300°C. The quadrupole mass spectrometer was operated in EI mode (70 eV), scanning between m/z 50–650 in 1 sec. The ion source temperature was 200°C.

[11] Sea surface temperatures (SST) were based on the alkenone unsaturation index, $U^{K'}_{37}$, which was calibrated to temperature with the equation ($U^{K'}_{37}$ = 0.033 * SST + 0.044) [*Prahl and Wakeham*, 1987]. Replicate injections and sample dilution tests allowed assessing measurement errors below 0.5°C [*Grimalt et al.*, 2001].

3. Chronological Framework

[12] A comprehensive description of the age model for PRAD1-2 was provided by *Piva et al.* [2008]. The borehole was ascribed to the last 370 ka, ranging from MIS 11.1 to MIS 1 (Figure 2). The proxies used to define the age model are summarized here.

3.1. Oxygen Stable Isotope Stratigraphy

[13] Two δ^{18}O records, obtained from the planktic foraminifer *G. bulloides* and from the benthic foraminifer *B. marginata*, allowed recognition of the most significant stratigraphic events (Marine Isotope Stages (MIS) and Terminations T I, T II and T III). The midpoints of T II and T III were taken as control points according to *Lisiecki and Raymo* [2005]. The midpoint of Termination I was not included as control point because of the higher resolution stratigraphy available in literature for this interval in the Adriatic Basin [*Asioli*, 1996; *Asioli et al.*, 1999; *Ariztegui et al.*, 2000]. Other additional control points, based on the ages of glacial stages and cold substages by *Martinson et al.* [1987] and *Bassinot et al.* [1994], were included for the interval older than MIS 5.1.

3.2. Biostratigraphy

3.2.1. Calcareous Nannoplankton

[14] Semiquantitative analysis allowed definition of two main bioevents: (1) the First Occurrence (FO) of *E. huxleyi* [*Rio et al.*, 1990] at 49.5 mbsf (264 ka according to *Lourens* [2004]); (2) a reversal in the dominance from *G. caribbeanica* to the group of small *Gephyrocapsa,* between 46.33 and 43.17 mbsf (260 and 245 ka according to *Villanueva et al.* [2002]). The age of the base of the borehole is younger than the Last Occurrence

(LO) of *Pseudoemiliania lacunosa* (in the sense of *Rio et al.* [1990]) occurring at 460 ka.

3.2.2. Foraminifera Bioevents

[15] Quantitative analysis provided the position of already well constrained bioevents, such as the LO of *Globorotalia inflata* at 6 ka B.P. and the LO of *Sigmoilina sellii* at 3 mbsf (circa 12.7 ka B.P. [14]C age, according to *Jorissen et al.* [1993]). New bioevents and their ages were defined by *Piva et al.* [2008], such as the entry of *S. sellii* at ∼12 mbsf (at 25.5 ka B.P. cal age), the Last Common Occurrence of *Hyalinea balthica* at 14 mbsf (28.3 ka B.P. cal age), the LCO of *G. inflata* at 16.9 mbsf within MIS 3 (43.1 ka B.P. cal age), the entry of *H. balthica* at 30.6 mbsf (124 ka B.P. cal age), the LO of *Islandiella islandica* at 31.2 mbsf (131 ka B.P. cal age) and the LO of *E. excavatum* forma *clavata* at 34.4 mbsf (162 ka B.P. cal age).

3.3. Magnetostratigraphy

[16] Two intervals with reverse polarity were identified at around 37 and 58 mbsf. Yet, only the former is well defined in both magnetic declination and inclination and could be used as control point. According to the $\delta^{18}O$ record, this excursion is positioned close to the MIS 7/6 boundary and correlates with the Iceland Basin Excursion (IBE), occurring around 188 ka B.P. [*Laj et al.*, 2006].

3.4. Radiocarbon Dates

[17] Six ^{14}C AMS dates (see *Piva et al.* [2008] for the complete list) were performed on benthic monospecific samples (*E. crispum* or *H. balthica*) at the Poznan Radiocarbon Laboratory, Poland, by using specimens from the size fraction >250 μm. These radiocarbon ages chronologically constrain two events: (1) the Last Glacial Maximum (19–23 cal ka B.P. according to the Chronozone defined by *Mix et al.* [2001]), located in PRAD1-2 between 10.3 and 7.7 mbsf, and (2) the LCO of *G. inflata* during MIS 3. This latter bioevent slightly predates the Campanian Ignimbrite tephra recognized by *Bourne* [2006] at 16.58–16.53 mbsf (and corresponding to TM-18 of *Wulf et al.* [2004]).

3.5. Sapropel Stratigraphy

[18] The dark and in some cases laminated sediment layers present in the borehole are characterized by extremely low values of $\delta^{18}O$ and $\delta^{13}C$ and by minima in concentration-related magnetic parameters (e.g., ARM), lower color reflectance [see *Piva et al.*, 2008] and by a characteristic foraminifera assemblage. Benthic foraminifera are present in most of these layers, except for two intervals (30.6–30.5 mbsf and 38.7–38.6 mbsf), where they are nearly absent. Where present, the benthic assemblage is generally dominated by taxa tolerating low-oxygen conditions such as *Bolivina*, *Brizalina*, *Fursenkoina* spp, *Chilostomella* (see ODS curve). Neogloboquadrinids (*Neogloboquadrina pachyderma* r. c. and *Neogloboquadrina dutertrei*) and/or *G. ruber* (pink variety) dominate the planktic assemblage, consistently with the literature [*Cita et al.*, 1977; *Rohling et al.*, 1993; *Negri et al.*, 1999; *Capotondi et al.*, 2006]. On he basis of these combined characteristics, ten dark layers present in PRAD1-2 borehole were considered as the central Adriatic equivalents of the deposition of eastern Mediterranean sapropels (and named S1 eq., S3 eq. and so on). The ages ascribed to these sapropel equivalents refer to the sapropel-based astronomical timescale established in the Ionian Sea, eastern Mediterranean, for the last 1.1 Ma by *Lourens* [2004].

3.6. Dansgaard-Oeschger Events

[19] A wiggle-match correlation between GISP2 ice core [*Meese et al.*, 1997] and PRAD1-2 $\delta^{18}O$ records within the last glaciation (latest MIS 5-MIS 2), integrated with lightness and XRF records (namely Ca/Ti and K/Ti ratios) allowed identification of Dansgaard-Oeschger events in PRAD1-2. These events provide additional control points and lead to a more refined age-depth model for the upper portion of PRAD1-2.

4. Results

4.1. Foraminifera

[20] The concentration on planktic and benthic foraminifera generally range between 200 and 1300 specimens per gram. Exceptions occur during the acmes of glacial stages 10, 8 and 2, which present near absent (MIS 10 and MIS 8) to low (MIS 2) planktic concentrations. Benthic foraminifera concentration is less than 50 specimens per gram during MIS 2. Tables 1 and 2 summarize the foraminifera assemblages characterizing PRAD1-2 cold and warm intervals, respectively, not including the assemblages present during the sapropel equivalent deposition.

[21] MIS 1 is rather condensed in PRAD1-2 record, compared to many other cores in the area and, in particular, to PRAD2-4, collected in 50 m

water depth on the shelf [*Cattaneo et al.*, 2006] and other published Adriatic cores [*Jorissen et al.*, 1993; *Asioli*, 1996; *Asioli et al.*, 1999, 2001; *Artizegui*, 2000; *Oldfield et al.*, 2003].

4.2. Stable Isotopes

[22] In addition to the general oscillatory trend reflecting the oxygen stratigraphy, the $\delta^{18}O$ *G. bulloides* curve (Figure 3) displays quite high values for glacial intervals with a general increasing trend of the values upward, from ~3.5‰ (MIS 9.2) to 4.5‰ (MIS 2). A similar trend is visible in the benthic $\delta^{18}O$ record (*B. marginata*), starting at MIS 7.4 (Figure 4). Moreover, the difference between the two curves ($\Delta\delta^{18}O_{B.\ marginata\text{-}G.\ bulloides}$) has been calculated and plotted in Figure 5 along with its 3 point smoothing curve. This proxy is considered here as an indicator of water mass stratification (the more the values increase, the more the water mass is stratified). Finally, the $\delta^{13}C$ benthic curve (*B. marginata*, Figure 9) shows high-amplitude oscillations (up to 1.5‰), while the main feature is the general increasing trend of the values of the glacial/cold intervals upward.

4.3. Alkenones

[23] The $U^{K'}_{37}$ SST record shows a broad range of variation (Figure 5), that follows the glacial-interglacial pattern with temperature values between 1–13°C and between 9–23°C during glacials and interglacials, respectively. The highest temperatures during interglacial intervals are similar to those encountered in the Holocene in the Gulf of Cadiz (22°C), Alboran (19°C) and Tyrrhenian (21°C) Seas [*Cacho et al.*, 2001]. In contrast, glacial periods exhibit much lower SST than those documented during MIS 2 in all the above mentioned Mediterranean basins [*Cacho et al.*, 2001]. In addition, strong cooling episodes are observed in PRAD1-2 within most glacial periods reaching SST values as low as 1°C (MIS 2 and 8), 3°C (MIS 3) or 5°C (MIS 4). The marked contrast between cold and warm SST implies very large temperature differences between glacial and interglacial stages, e.g., as much as about 16°C between MIS 10 and 9, 8 and 7, and 2 and 1, and as much as 19.5°C between MIS 6 and 5.

5. Discussion

5.1. PRAD1-2 General Climate Trends

[24] PRAD1-2 interglacial and interstadial intervals are characterized by flux peaks of warm-water planktic foraminifera species (Figure 5), paralleled by significant shifts in the oxygen stable isotope and alkenone-derived SST curves. MIS 5.5 appears as the warmest substage of the entire record (about 22°C) and is characterized by the presence of subtropical planktic dweller *G. sacculifer*. Similarly high SST values are found in interglacials MIS 7 and 9. Most glacial-interglacial transitions exhibit rapid and large SST increases, as for the 19.5°C warming during Termination II (Figure 5). During interglacial intervals, temperature changes record stadial-interstadial oscillations with maxima during stages 5.1, 5.3, 5.5, 7.1, 7.3, 7.5, 9.1 and 9.3 (Figure 6), as on the western Iberian and Alboran margins [*Martrat et al.*, 2004, 2007].

[25] An overall cooling trend characterizes both MIS 9 and MIS 5, while MIS 7 shows the opposite. Substages 7.3 and 7.1 are warmer than MIS 7.5, on the basis of both SST values and the planktic assemblage composition (occurrence of the subtropical species *G. sacculifer* during MIS 7.3 and 7.1). This succession of climatic changes matches with the integrated sea-land records (marine and pollen data) described by *Tzedakis et al.* [2004], *Roucroux et al.* [2007], and *Desprat et al.* [2006, 2007] on the western Iberian margin. These authors suggested an insolation maximum during MIS 7.3 similar to the one in MIS 7.5 and a mild stadial of MIS 7.2, the latter characterized by reduced ice caps compared to the other stadials [*Shackleton*, 2000], and by only a slight decrease of Atlantic sea-surface temperatures [*McManus et al.*, 1999].

[26] The planktic foraminifera assemblage indicates dominant oligotrophic conditions in the surface water during warm intervals. Higher productivity conditions, either related to the development of a Deep Chlorophyll Maximum (peaks of Neogloboquadrinids) or concentrated in the uppermost water column (abundant *G. quinqueloba* and/or *G. bulloides*), mainly correspond to the deposition of sapropel equivalent layers. *G. inflata*, a winter deep dweller species requiring vertical mixing and a cool and homogeneous water column [*Pujol and Vergnaud Grazzini*, 1995], is generally present during warm substages and also at the onset and/or at the end of cold substages (5.4 and 7.4), but not during the deposition of sapropel equivalents, confirming the strong stratification of the water mass during these events. Therefore, when present, *G. inflata* can be considered an indicator of deep water production, assuming that during past interglacials and interstadials the northern Adriatic deep-water formation occurred through mecha-

Table 1. Microfaunistic Characterization of the Foraminifera Assemblages During the Main Cold Oscillations Registered in PRAD1-2 Record

Marine Isotope Stages	Planktic Foraminifera	Benthic Foraminifera
MIS 10	near-absent	overall homogeneous assemblage; abundant *Bulimina* ex gr. *marginata* and common *Ammonia perlucida* in the late MIS
MIS 8	very few specimens, mostly belonging to *G. quinqueloba*	extremely oligotypic assemblage, dominated by *Islandiella islandica* and *Elphidium articulatum*
MIS 6	*G. quinqueloba* still dominant with scattered presence of *G. ruber* and *G. bulloides*; very rare *Neogloboquadrina pachyderma* left coiled in the upper part of the stage	assemblages with alternating dominance of *Cassidulina laevigata carinata*, *I. islandica* and *Elphidium* spp (mainly *E. articulatum* and *Elphidium exacavatum* forma *clavata*)
MIS 4	strong dominance of *G. quinqueloba*	*C. laevigata carinata* very frequent (about 50%), with common to abundant *Hyalinea balthica* (this is the only glacial stage in which *H. balthica* occurs in the Adriatic record)
MIS 2	*G. quinqueloba* dominant, with rare *G. bulloides* and very rare *G. ruber*	alternating peaks of *C. laevigata carinata*, *Elphidium crispum* and *Elphidium decipiens*; deep infaunal *Glandulina laevigata* abundant in two distinct levels (5.88 and 11.60 mbsf)
Substages MIS 9.2, MIS 7.4, MIS 7.2, MIS 5.4, and MIS 5.2	assemblage generally dominated by *G. quinqueloba*, along with common to abundant *G. bulloides* (in particular during MIS 7.4 and MIS 5.2)	dominance of *C. laevigata carinata* accompanied by *E. decipiens* and *E. crispum*

Table 2. Microfaunistic Characterization of the Foraminifera Assemblages During the Main Warm Oscillations Registered in PRAD1-2 Record

| Marine Isotope Stages	Planktic Foraminifera	Benthic Foraminifera
MIS 11	warm species present (*G. ruber*, *Orbulina*); *Globorotalia inflata* common to abundant	*C. laevigata carinata* dominant along with *B.* ex gr. *marginata*.
MIS 9	common warm species (*G. ruber*, *Orbulina*, *Z. rubescens*) in non-sapropelic levels with common *G. inflata*	*C. laevigata carinata* abundant with *B.* ex gr. *marginata*; *Cibicidoides pachyderma* shows a distinctive peak at 53.5 mbsf
MIS 7	common to abundant warm species (*G. ruber*, *Orbulina*, *Z. rubescens* and *Globigerinoides sacculifer* (MIS 7.3 and 7.1)); *G. inflata* present along with scattered presence of *Globorotalia truncatulinoides*; *G. inflata* dominates MIS 7.1.	*C. laevigata carinata* abundant (dominant during MIS 7.5); infaunal species (*Brizalina*, *Bolivina*, *Bulimina* and *Uvigerina*) common; *Trifarina angulosa* and *C. pachyderma* common in all the three substages.
MIS 5	common to abundant warm species (*G. ruber*, *Orbulina*, *Z. rubescens* and *G. sacculifer* (MIS 5.5)); *G. inflata* common in MIS 5.3 and 5.1	reversal in the frequencies of *C. laevigata carinata* + *H. balthica*, increasing upward during MIS 5; decrease of *Brizalina*, *Bolivina*, and *Uvigerina* groups; *B.* ex gr. *marginata* is common in the three warm oscillations, as well as *T. angulosa* and *C. pachyderma*.
MIS 3	warm assemblage with *Orbulina* and *G. ruber*; *G. inflata* rare to common	alternating levels of abundant *C. laevigata carinata* and *H. balthica*; *T. angulosa* common in the lower part of the stage
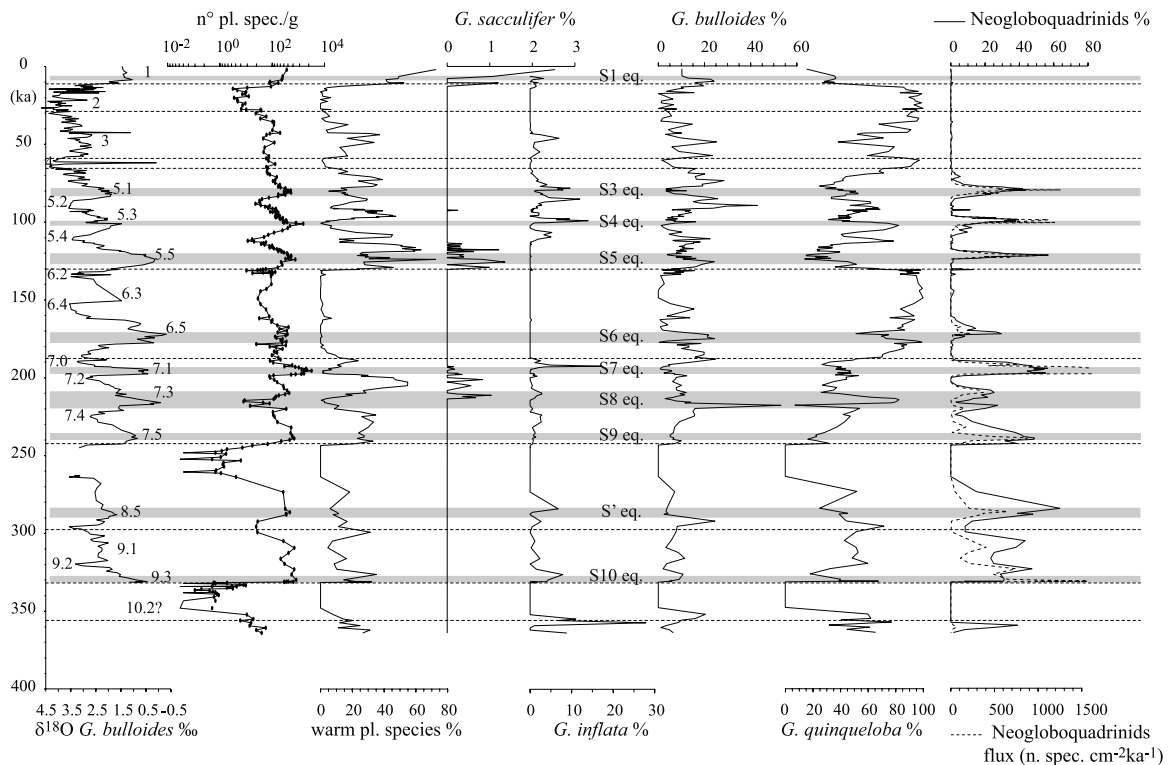
Figure 3. Records of the main planktic foraminifera species. On the left, the $\delta^{18}O$ record of *G. bulloides* is reported as well as the concentration of the planktic foraminifera (number of specimens per gram of dry sediment; note the logarithmic scale). All the species are expressed as percentages, while the flux of Neogloboquadrinids (dotted line) is expressed as number of specimens per area unit (cm²) per time unit (ka). Neogloboquadrinids include *N. pachyderma* and *N. dutertrei*. Grey areas indicate sapropel equivalent levels.

nisms similar to the modern interglacial [*Artegiani et al.*, 1997; *Lascaratos et al.*, 1999].

[27] The difference between planktic and benthic foraminifera oxygen isotope values ($\Delta\delta^{18}O_{B.\ marginata} - \delta^{18}O_{G.\ bulloides}$) is an indicator of the water mass homogeneity. When Δ values approach zero the water mass tends to become more uniform, while increasing Δ values reflect a stronger stratification of the water column. Consistently, the $\Delta\delta^{18}O$ curve for PRAD1-2 (Figure 5) shows the highest values (up to about 2.5‰) during the deposition of the Adriatic sapropel equivalent layers, while minima in $\Delta\delta^{18}O$ are mainly recorded during cold intervals. *G. inflata* is absent during the acme of glacial intervals (MIS 10.2, 8.4, 6), when $\Delta\delta^{18}O$ minima are extreme and the water depth was too shallow to allow the appropriate depth habitat of this intermediate water dweller.

[28] Excluding the sapropel-equivalent intervals, the benthic assemblage indicates an upper slope mesotrophic environment during all interglacials and interstadials, characterized by the accumulation of organic matter on the seafloor and relatively low oxygenation. However, in this mesotrophic environment a small amount of epifaunal species, like *C. pachyderma* and *T. angulosa*, is indicative of well oxygenated bottom waters. This occurrence therefore suggests seasonal bottom ventilation, comparable with modern conditions, characterized by winter production of oxygenated, dense water in the north Adriatic.

[29] Glacial stages show distinctive features both in terms of paleodepth and climate trends. MIS 10 shows the shallowest glacial sea level of the whole borehole, as testified by the near-absence of planktic foraminifera and by the high percentage of *Elphidium* + *Ammonia*. More in detail, the presence of *A. perlucida,* inhabiting the muddy coastal zone of the modern Adriatic [*Jorissen*, 1988] reflects a very shallow environment (*A. perlucida* is dominant in <10 m, according to *Morigi et al.* [2005]) characterized by fresh water runoff. In contrast, MIS 4 is characterized by the deepest glacial basin conditions, with higher total planktic foraminifera flux and it is dominated by *C. laevigata carinata*. Some PRAD1-2 glacial intervals are characterized by the presence, or the
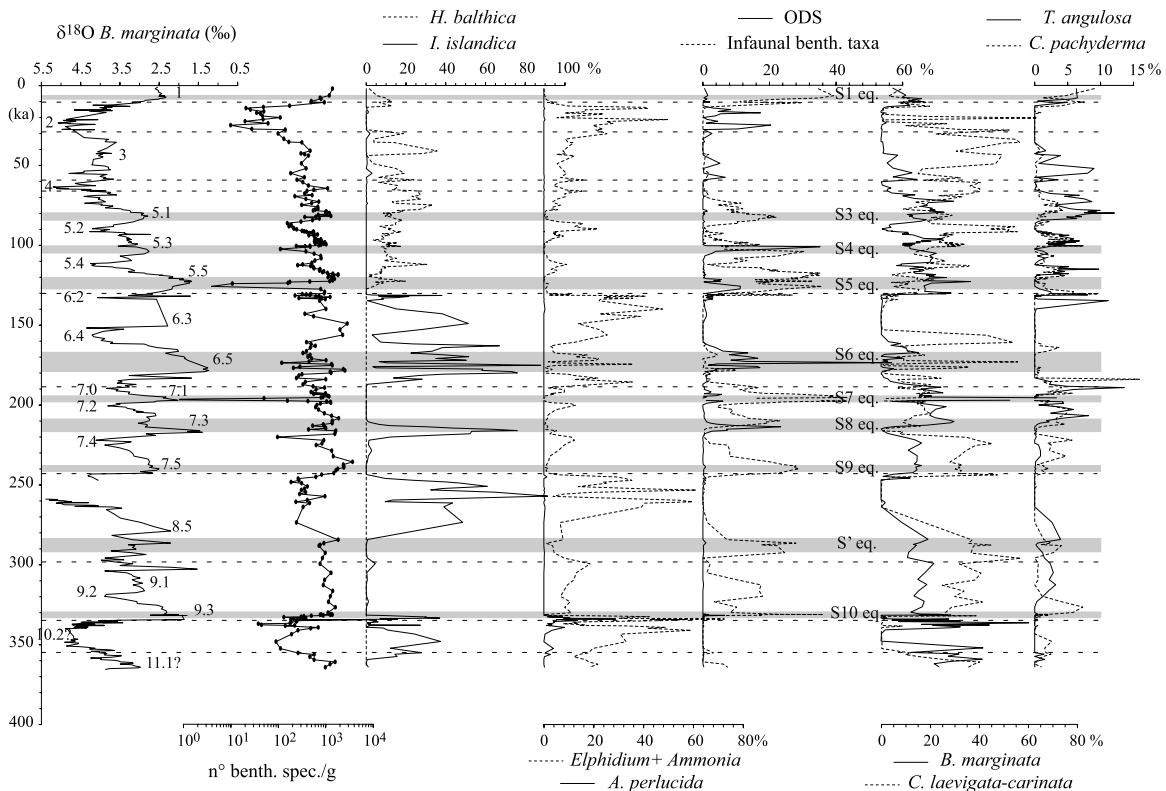
Figure 4. Records of the main benthic foraminifera species. On the left the $\delta^{18}O$ record of *B. marginata* is reported as well as the concentration of the benthic foraminifera (number of specimens per gram of dry sediment; note the logarithmic scale). All the species are expressed as percentages. Grey areas indicate sapropel equivalent levels.

dominance, of peculiar benthic foraminifera species presently living outside the Mediterranean, at higher latitudes:

[30] 1. *I. islandica* is presently abundant in Arctic areas and in northern European fjords, living at temperature <10°C [*Murray*, 2006]; in PRAD1-2 this species peaks during glacial MIS 6, 8 and 10, as well as during the deposition of cold sapropel equivalent S8. The SST record of PRAD1-2, although referred to more surficial waters, is consistent with the temperature range required by *Islandiella*.

[31] 2. *E. excavatum* forma *clavata* is an opportunistic species [*Linke and Lutze*, 1993], abundant in high-latitude fjords and estuaries [*Miller et al.*, 1982] sometimes close to glaciers and meltwaters [*Murray*, 2006; *Alve*, 1995] in cold climate environment [*Wilkinson*, 1979; *Rodrigues and Hopper*, 1982; *Williamson et al.*, 1984; *Jennings et al.*, 2004]. In PRAD1-2 this species is present within MIS 10 and 6, during the shallowest and river-influenced conditions recorded by the whole sequence and within Sapropel 6 equivalent layer,

respectively, both implying reduced-salinities in surface waters.

[32] *S. sellii* is present in PRAD1-2 record only during MIS 2, as already reported by *Jorissen et al.* [1993] and *Asioli* [1996] for the Adriatic Sea.

5.2. Comparison With Other Records

5.2.1. Western Mediterranean

[33] We compare PRAD1-2 $\delta^{18}O$ *G. bulloides* and alkenone-derived SST records to the time equivalent succession from ODP Site 977A (Figure 1), the western Mediterranean Sea record with the highest resolution for the last 250 ka [*Martrat et al.*, 2004].

[34] The $U_{37}^{k'}$ SST record reported by *Martrat et al.* [2004] for the Alboran Sea (Figure 6) indicates SSTs quite similar to those reported during warm substages in PRAD1-2. Intervals of abrupt warming are detected in PRAD1-2 by concurrent peaks of $\delta^{18}O$, SST and warm planktic foraminifera (flux and frequency) in particular during MIS 9.3 (12°C shift), 9.1 (7°C), 7.5 (13°C), 5.5 (18.5°C) and 1
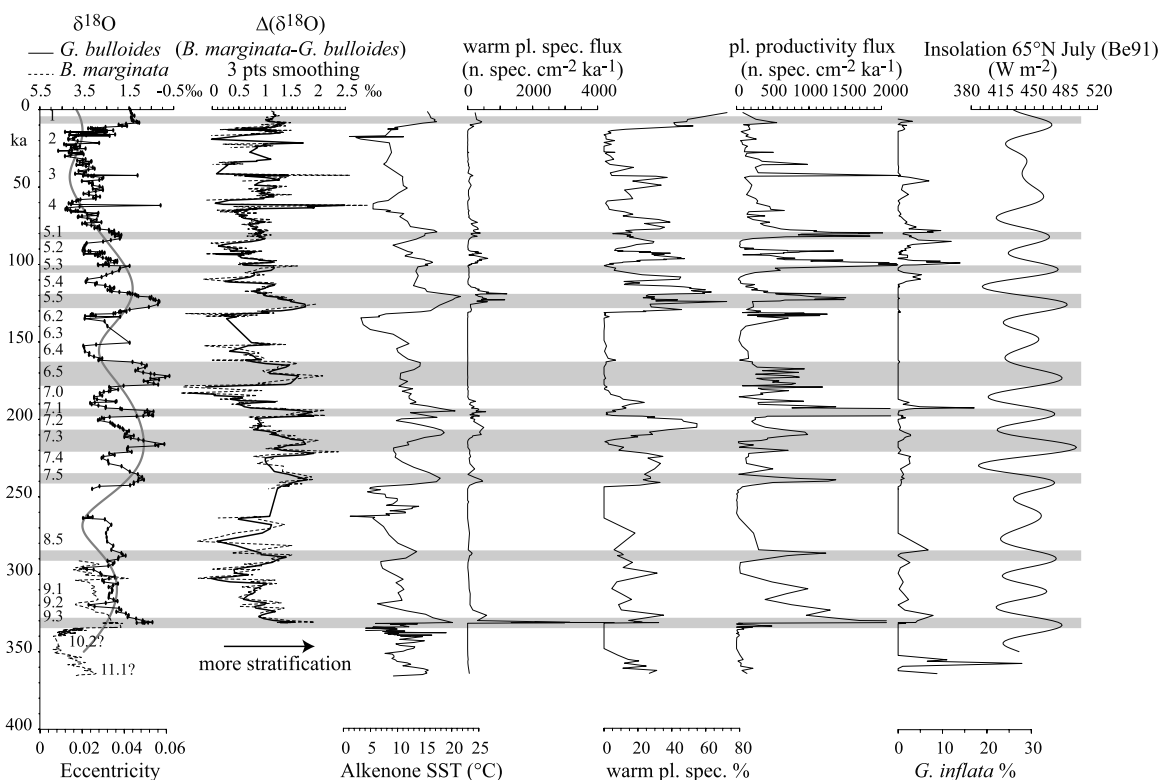
Figure 5. Synthesis of the main proxies of borehole PRAD1-2 against insolation (Be91 from *Berger and Loutre* [1991], rightmost plot) and eccentricity (Be91, leftmost plot). The alkenone-derived SST parallels significantly the $\delta^{18}O$ records.

(8°C), confirming the conclusion made by *Martrat et al.* [2004] that cold stadials had only limited duration, immediately followed by well-defined returns to interstadials with accelerated warming by positive feedback mechanisms once a threshold was passed. However, PRAD1-2 reveals several exceptions, with regard to the exact timing of the highest SST values, in turn affecting the duration of some warm interstadials. Indeed, maximum warming is differently recorded by $U^{k'}_{37}$ SST or warm planktic foraminifera frequency. In detail, frequency peaks of warm planktic species and minima of $\delta^{18}O$ values are not in phase with coeval peaks of $U^{k'}_{37}$ SST and warm planktic flux. These phase lags seem to reflect decrease in productivity (see the planktic productivity flux curve in Figure 5) before or after the maximum $U^{k'}_{37}$ SST, producing a poorer total flux of planktic foraminifera assemblage but a relative increase in warm species. An example of this discrepancy is MIS 5.3, a warm substage including two stable warm intervals, Alboran Interstadials 24 (AI24) and 23 (AI23) in the western Mediterranean [*Martrat et al.*, 2004], separated by the abrupt cold oscillation Alboran Stadial 24 (AS24) (Figure 6). In PRAD1-2, warm planktic

species flux as well as $U^{k'}_{37}$ SST record show a small increase at the base of AI24, while the frequency of warm planktic species clearly defines a warming at the base of this substage (circa 109–110 ka). This latter increase in frequency co-occurs with a drop in productivity. A similar feature can be observed for the base of MIS 5.1 in PRAD1-2, compared to the Alboran site. The PRAD1-2 $U^{k'}_{37}$ SST record reaches its maximum just after the end of Sapropel 3 equivalent, delaying the timing of the maximum warmth of this substage.

[35] All these observed trends lead to the conclusion that the Adriatic basin is not capable to maintain interglacial and interstadial conditions with a duration similar to the western Mediterranean and eastern Atlantic [*Martrat et al.*, 2004, 2007], as suggested by three observations: (1) during MIS 7.3, 7.1, 5.3 and 5.1, the decreasing SST trend toward cold substages starts earlier in the Adriatic Basin than in the Alboran Sea; (2) similarly, the subsequent SST increase in warm substages is slower and delayed in PRAD1-2, resulting in prolonged intervals with low SST; and (3) in PRAD1-2 the maximum $U^{k'}_{37}$ SST within MIS 7.3 is achieved later.
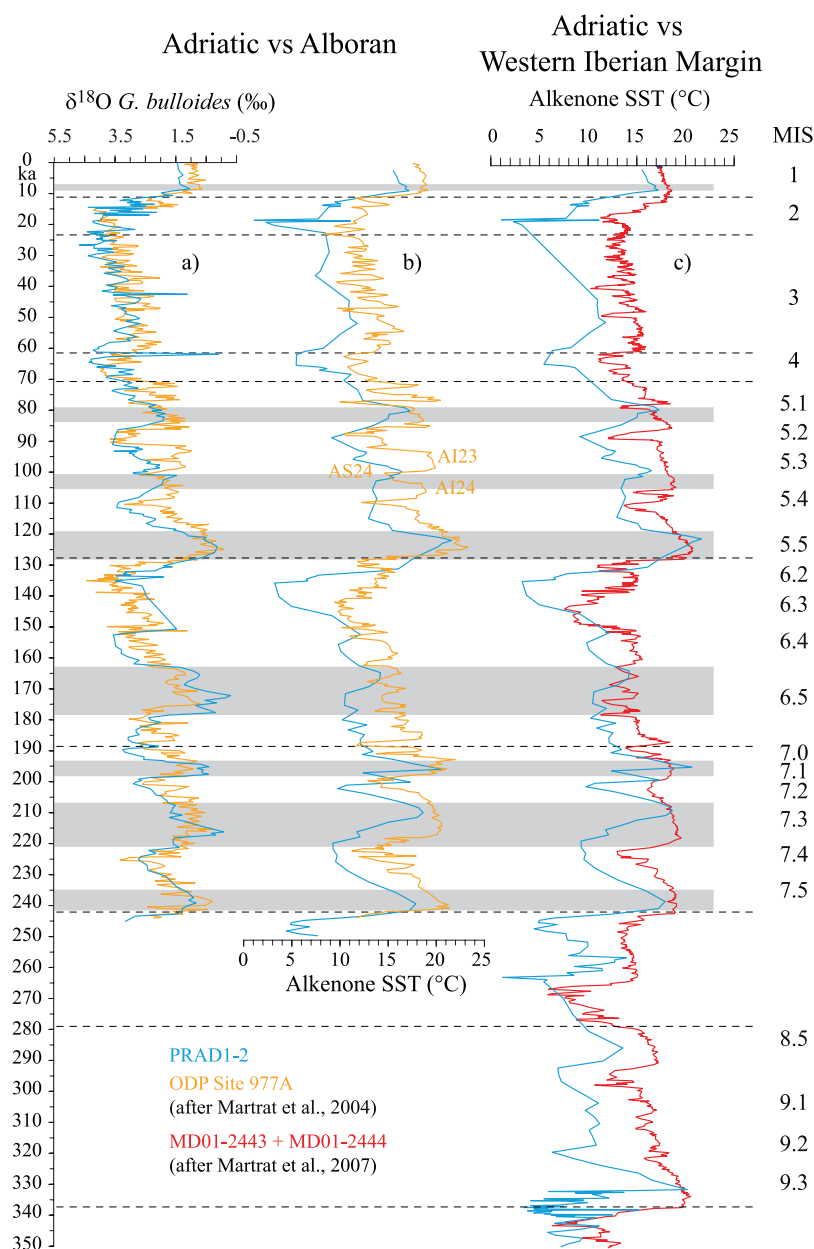
Figure 6. (a) Comparison between δ^{18}O *G. bulloides* records of the last 250 ka of the ODP site 977A (Alboran Sea [*Martrat et al.*, 2004]) and PRAD1-2 records. (b) Comparison between $U_{37}^{k'}$ SST records of the ODP site 977A [*Martrat et al.*, 2004] and PRAD1-2. ODP 977A records (yellow) are plotted according to the age-depth model by *Martrat et al.* [2004]. (c) Comparison between $U_{37}^{k'}$ SST records of the composite western Iberian site (red line) by *Martrat et al.* [2007] and of PRAD1-2 (blue line). Grey areas indicate the sapropel equivalent layers detected in PRAD1-2, and horizontal dashed lines denote MIS boundaries.

[36] The overall very low SST, uncommon for the Mediterranean Sea, and the shorter duration of warm intervals documented for the Adriatic, may be explained by three interacting causes, which are here listed on the basis of their inferred relative importance: (1) the landlocked nature of this shallow basin, especially during the glacial stages, when sea level was more than 100 m lower than at present, probably amplified the SST excursion and increased the atmospheric forcing, e.g., through outbreaks of northerly polar continental air masses (Siberian High), as already argued by *Rohling et al.* [2002] for the Holocene cold oscillations; (2) the vicinity of the basin to large Alpine and Apennine glaciers, conveying cold air, an uncommon condition for the Mediterranean; and

(3) the location at a latitude at least 3° higher than the best documented Mediterranean sites. The South China Sea semienclosed basin is one of the few continental margin settings with a geomorphology similar to the Adriatic and strongly affected by sea level changes impacting its broad shelves, emerged during glacial stages. From this enclosed basin, *Pelejero et al.* [1999a, 1999b] reported $U_{37}^{k'}$ SST excursions between LGM and Holocene 1–3° higher than those observed at the same latitudes in the Atlantic and Pacific Oceans, and suggested that the influence of the continental climate changes on the nearby marine system could act as amplification mechanism increasing the glacial/interglacial differences in that marginal sea. This mechanism has been explained with sea level fluctuations that permitted or prevented surface seawater exchange with the tropical Indo-Pacific waters [*Pelejero et al.*, 1999a].

[37] Glacial intervals like MIS 10, 8.4, 6.2 and 2 experienced the lowest temperatures (2–4°C) and MIS 4 was just slightly warmer (5°C). These central Adriatic SST are typically 3–4°C lower than at the Alboran site [*Martrat et al.*, 2004] both during glacial and stadial intervals (Figure 6). Greatest SST differences (up to 5–7°C) between the two sites are recorded during MIS 6.2–6.3, MIS 4 and MIS 2. The comparison of the SST record between PRAD1-2 and the Iberian Margin [*Martrat et al.*, 2007] for the last four climate cycles confirms differences as recognized between the Alboran and Adriatic Sites also for MIS 8 as well as for the interstadials MIS 9.1 and 9.3 (Figure 6).

[38] During MIS 6, the Adriatic and Alboran records show a similar planktic $\delta^{18}O$ record, but the Adriatic displays higher values during stadial 6.4 and slightly lower values during 6.5. These lower values, as well as more frequent $\delta^{18}O$ oscillations during MIS 6.5, can be explained in PRAD1-2 with the presence of Sapropel 6 equivalent, considering that this sapropel is composed by multiple phases both in the eastern Mediterranean [*Schmiedl et al.*, 1998; *Jorissen*, 1999; *Casford et al.*, 2003] and in the central Adriatic (see peaks of planktic productivity flux curve in Figure 5). The possibility that also the closely spaced $\delta^{18}O$ oscillations documented in the Alboran Sea between 165 and 180 ka reflect to some extent the establishment of conditions leading to sapropel formation cannot be ruled out. The SST records of the two sites are quite different. In fact, according to *Martrat et al.* [2004], the Alboran Sea displays a millennial scale variability during MIS 6, while

PRAD1-2, although with much lower resolution, shows consistently lower SST during the earlier part of MIS 6.5. Interestingly, the lowest values of SST correspond to low $\delta^{18}O$ values and probably reflect intervals of enhanced runoff of cold riverine waters.

[39] The chronology adopted for borehole PRAD1-2 allows some inferences about the timing of Sapropels 4 and 8. Sapropel 8 equivalent, already recognized as a typical "cold sapropel" [*Cita et al.*, 1977; *Vergnaud-Grazzini et al.*, 1977; *Emeis et al.*, 1998; *Lourens*, 2004] occurs at the base of MIS 7.3 in PRAD1-2 record, above the highest $\delta^{18}O$ peak of MIS 7.4, as recorded also by *Schmiedl et al.* [1998] and by *Emeis et al.* [2003] in deeper-water settings, and not in the early phase of MIS 7.4 [*Lourens*, 2004]. PRAD1-2 S8 equivalent is characterized by $U_{37}^{k'}$ SST of ~12°C, colder than the $U_{37}^{k'}$ SST estimate (12 to 16°C) by *Emeis et al.* [1998, 2000a] for the Levantine Basin. These low temperatures may reflect cold surface water produced by enhanced runoff (low $\delta^{18}O$ values) during the first phase of the S8 equivalent layer, followed by an increase of planktic productivity along with an increase of $U_{37}^{k'}$ SST and warm planktic species flux. Only after the sharp drop in planktic productivity flux the warm species percentage peaks, lagging behind the $U_{37}^{k'}$ SST peak.

[40] Sapropel 4 equivalent seems to be coeval to the cold oscillation AS24, registered in the Alboran site. An equivalent cold episode, lasting 2–4 ka and interrupting MIS 5.3 has been also detected by *Desprat et al.* [2007] on the western Iberian margin. Moreover, the Organic Rich Layer 6 (ORL6), recognized during MIS 5 in the ODP site 977 has been dated by *Perez-Folgado et al.* [2004] at 100.3–102.3 ka B.P. (well matching with the age of 101 ka established by *Lourens* [2004] from astronomical tuning) and related to an early phase of Sapropel 4. The ORL6 is stratigraphically positioned in the oxygen isotope record on the shift leading to the cold spell labeled AS24 by *Martrat et al.* [2004]. Therefore the relatively low SST of the Sapropel S4 equivalent in PRAD1-2 can be explained by its occurrence during the AS24 cold spell, even if its development is associated to an isolation maximum [*Lourens*, 2004]. This is in agreement with the conclusion made by *Emeis et al.* [1998] that SST in sapropels are not related only to insolation and do not directly reflect warming from radiation during the last 500 ka. Instead, their baseline temperature is related to global ice volume, possibly through cooling from inland glaciers

and lowered snow lines in the northern Mediterranean watershed. A shift in the bloom season of the coccolith *E. huxleyi* is a complementary explanation for the low SST recorded during S4; such a shift would have been triggered by a change in the structure of the water column during its winter and spring growing season in the Mediterranean [*Knappertsbusch*, 1993; *Totti et al.*, 2000]. Similar shifts in the growth season have already been suggested for Sapropel 1 by *Sangiorgi et al.* [2003] and in the open ocean by *Chapman et al.* [1996] and *Weldeab et al.* [2007].

5.2.2. Eastern Mediterranean

[41] *Sanvoisin et al.* [1993] analyzed the oscillations in the planktic foraminifera assemblage in the Ionian Basin. Core KC01-B was retrieved in 3643 m water depth (Figure 1), and spans the last circa 1100 ka B.P. The correlation between PRAD1-2 record and the last circa 340 ka B.P. of the Ionian core allowed the identification of major similarities and differences between the two basins, reflecting local processes in the Adriatic region (Figure 7). Although different sieve meshes were adopted (150 μm for core KC01-B versus 106 μm for borehole PRAD1-2), the correlation between the two records can be attempted, on the basis of the main trends of foraminifera distribution. *Asioli et al.* [2001] reported common trends in planktic foraminifera records comparing sequences from central, southern Adriatic, Tyrrhenian and Ionian sites even if studied with different sieve meshes of 63 μm versus 125 μm. Similarly, *Capotondi et al.* [2006] reported common trends and bioevents successions among cores studied on fraction either >63 μm or >150 μm in size.

[42] Warm planktic species in core KC01-B allow, despite the lower stratigraphic resolution, recognition of all the major warm oscillations documented in the more detailed PRAD1-2 record, in particular for MIS 5 and MIS 7. Subtropical planktic dweller *G. sacculifer* displays a consistent trend, peaking during MIS 5.3, 5.5, 7.1 and 7.3, characterizing these intervals as the warmest in the investigated interval. Moreover, the planktic deep-dweller *G. truncatulinoides*, which requires a well developed winter vertical mixing, peaks in both records during MIS 5.1, 5.3, 7.1, 7.5 and 9.3, suggesting an enhanced seasonal contrast during these interstadials. Consequently, during MIS 5.5 and MIS 7.3, these data suggest a prolonged summer warm season and a weaker winter cooling, consistently with the 65°N summer insolation and eccentricity index curves. MIS 5.3 and 7.1 display warm

summer conditions, along with a well developed winter vertical mixing, suggesting an improved seasonal contrast. MIS 5.1, MIS 7.5 and MIS 9 in PRAD1-2 appear to be relatively cold. The Ionian record, instead, brings evidence of warm climate conditions (peaks of *G. sacculifer*) also earlier than MIS 7.3. Consequently, it seems that the climatic evolution of the two areas particularly matched within the time interval from MIS 7.3 to MIS 5.3. This interpretation is also supported by the oxygen stable isotope data, indicating a higher intensity of sapropel-equivalent events from S8 to S4. This interpretation is reinforced by the presence of deep infaunal taxa only during these sapropel equivalent beds (ODS curve) and suggests that in the time interval between S8 and S4 the conditions of the central Adriatic were more similar to those of the eastern Mediterranean, at least during the sapropel deposition. Several mechanisms have been proposed to explain the formation of sapropel layers: anoxia, productivity increase, large-scale fluvial input linked to the increase of the intensity of the African monsoon season [*Rossignol-Strick et al.*, 1982; *Rossignol-Strick*, 1983; *Emeis et al.*, 2000b, 2003] (see also *Cramp and O'Sullivan* [1999] and *Meyers* [2006] for reviews) or of the Indian Ocean summer monsoon [*Rohling*, 1994]. Considering these possible mechanisms, the stronger surface water dilution along with the relatively large thickness of PRAD1-2 sapropel-equivalent intervals S8 to S4 (typically 50 to 100 cm each) suggest enhanced precipitation over the central Adriatic brought about by a stronger influence of the monsoon system over the Mediterranean. The Adriatic and Ionian microfaunistic records differ more significantly during glacial intervals than during interglacials, but this fact is mainly a consequence of the shallow depth of the central Adriatic where sea level falls hampered the intrusion of deep-dwelling planktic taxa leaving a planktic association dominated by shallow- and intermediate-water dwellers, as *G. quinqueloba* and *G. bulloides*.

5.2.3. Bottom Water Formation

[43] Figure 8 shows a comparison of the PRAD1-2 planktic and benthic δ^{18}O records with their planktic counterparts in the Ionian Basin (core M25/4-KL13 [*Schmiedl et al.*, 1998]), eastern Mediterranean, and in the Balearic abyssal plain (ODP Site 975 [*Pierre et al.*, 1999]), western Mediterranean. A third planktic δ^{18}O record, from the North Atlantic (ODP Site 980 [*McManus et al.*, 1999]), is far from any Mediterranean paleoceano-
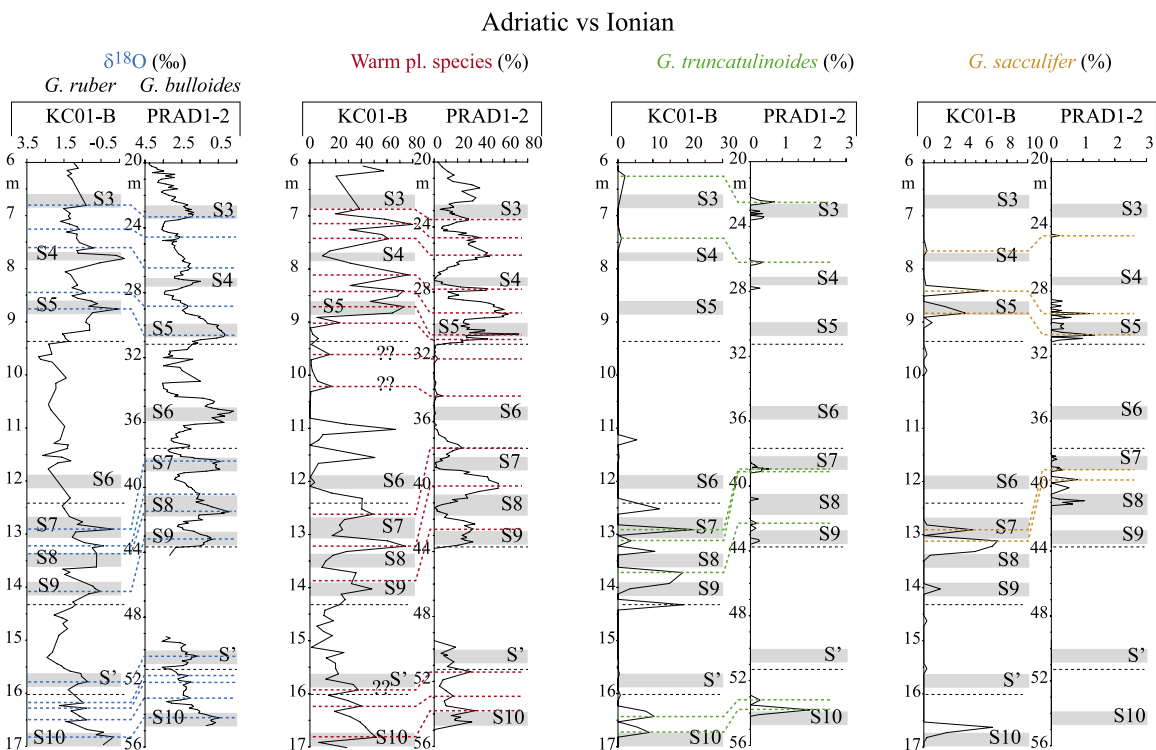
Figure 7. Comparison between frequency plots of selected planktic species from KC01-B (Ionian Sea [*Sanvoisin et al.*, 1993]) and PRAD1-2 records. Oxygen record of *G. ruber* from *Langereis et al.* [1997] is also reported for core KC01-B. Grey areas denote the sapropel equivalent layers in PRAD1-2 and the sapropels present in core KC01-B [*Langereis et al.*, 1997]. Horizontal black dashed lines indicate MIS boundaries.

graphic peculiarity such as those leading to the deposition of sapropels. All the Mediterranean $\delta^{18}O$ curves are on *G. bulloides* (no correction for vital effects or ice volume was applied) while the North Atlantic record is on *N. pachyderma* r. c. PRAD1-2 record shows comparable glacial values during MIS 8 and MIS 6 (3.5‰), following a shift toward higher values in MIS 4 (4.3‰) and in MIS 2 (up to 4.6‰). Over the last 350 ka, these values are high, also when compared with $\delta^{18}O$ *G. bulloides* records of the North Atlantic (not shown). Atlantic cores collected between 37 and 42°N latitudes and comparable to PRAD1-2 site (CH69-K09 by *Labeyrie et al.* [1999] and the composite record off Iberia by *Desprat et al.* [2007]) indicate $\delta^{18}O$ values not higher than 3‰ during glacial stages with no long-term trend. The Ionian and North Atlantic sites show a trend similar to the Adriatic, except for lower values during MIS 4, where $\delta^{18}O$ values on *G. bulloides* overlap the $\delta^{18}O$ record obtained on deeper dweller *N. pachyderma* r. c. On the contrary, in the Balearic site the glacial stages from MIS 8 to MIS 2 are characterized by values around 3.5‰, indicated by the almost vertical yellow arrow in Figure 8. This

comparison suggests that up to MIS 6 surface waters in Adriatic were similar to the other central Mediterranean sites, but after MIS 6, and mainly during MIS 2, the Adriatic and the Ionian basins were probably more influenced by northerly, polar, continental-air outbreaks during glacial stages.

[44] The $\delta^{18}O$ *G. bulloides* gradient in PRAD1-2, paralleled by the $\delta^{18}O$ *B. marginata* one (green curve), suggests that, starting from MIS 6, and possibly already from MIS 7.4, surface and bottom waters record a decrease in temperature and/or an increase in salinity both during glacial and stadial intervals. The $U_{37}^{k'}$ SST record indicates quite low temperatures (below 5°C) for glacial MIS 6, 4 and 2, while SST estimates are 10–14°C for stadial MIS 5.2 and MIS 5.4. For this reason we cannot rule out a component of high salinity behind the high $\delta^{18}O$ values, beside the ice-volume component. Only the benthic foraminifera $\delta^{18}O$ record seems to support the presence of cold and saline bottom waters since MIS 5, because the cold water shelf benthic species *H. balthica* shows increases along with *C. laevigata carinata*, an epifaunal benthic species related to normal [*Van der Zwaan and Jorissen*, 1991] to high [*Vilks*, 1989] bottom
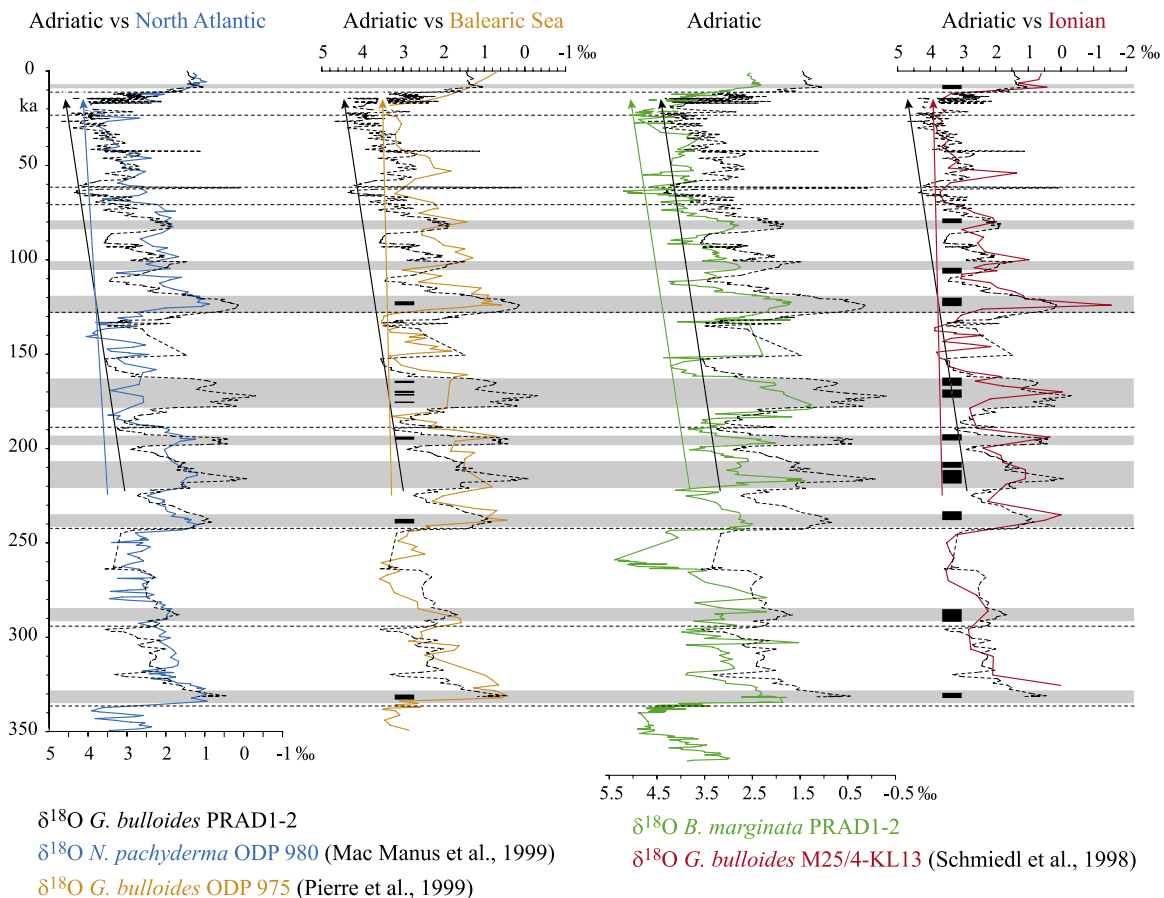
Figure 8. Correlation of PRAD1-2 planktic δ^{18}O record (dashed line) with records from the North Atlantic (first plot), the Balearic sea (second plot) and the Ionian sea (fourth plot). Grey areas denote PRAD1-2 sapropel equivalent layers, whereas black areas beside each graph refer to the organic-rich layers found in the other Mediterranean records. Arrows indicate the isotopic trend toward higher glacial-interval values.

water salinity (Figure 9). These parameters may indicate that the production of dense water progressively increased in the central Adriatic since MIS 6 and up to MIS 2. Accordingly, the ODS curve (Figure 4) suggests low ventilation intervals only in correspondence of sapropel equivalent layers and during two short-lasting stagnation events (peaks of *G. laevigata*) during MIS 2 (according also to the benthic record of other central Adriatic cores [*Asioli*, 1996]). Moreover, the overall trend of δ^{13}C of *B. marginata*, reaching the lowest values in correspondence of the sapropel-equivalent beds, appears to become progressively higher upward and with high values in correspondence of glacial and stadials intervals, confirming a good ventilation (Figure 9). *Cacho et al.* [2006] carried out a quantitative study on deep water production in western Mediterranean for the last 50 ka and demonstrated that the densest (saltiest) waters

formed during MIS 2 and during D-O stadials. Our observations confirm these conclusions and extend them over a longer interval (250 ka).

[45] *Myers et al.* [1998] made three modeling experiments to reconstruct the LGM Mediterranean circulation. Despite the different boundary conditions, all models show no evidence of deep water formation in the Adriatic Sea. Under these conditions, deep water formed solely in the Levantine basin ventilating the deep Ionian [*Schmiedl et al.*, 1998]. The new data from PRAD1-2 suggest, instead, that this scenario may not be representative of glacial and stadial intervals older than the LGM (and likely not even for the entire MIS 2), as the central Adriatic shallow basin may have contributed to the deep-water formation through the formation of very cold and dense water spilling over the Pelagosa sill,
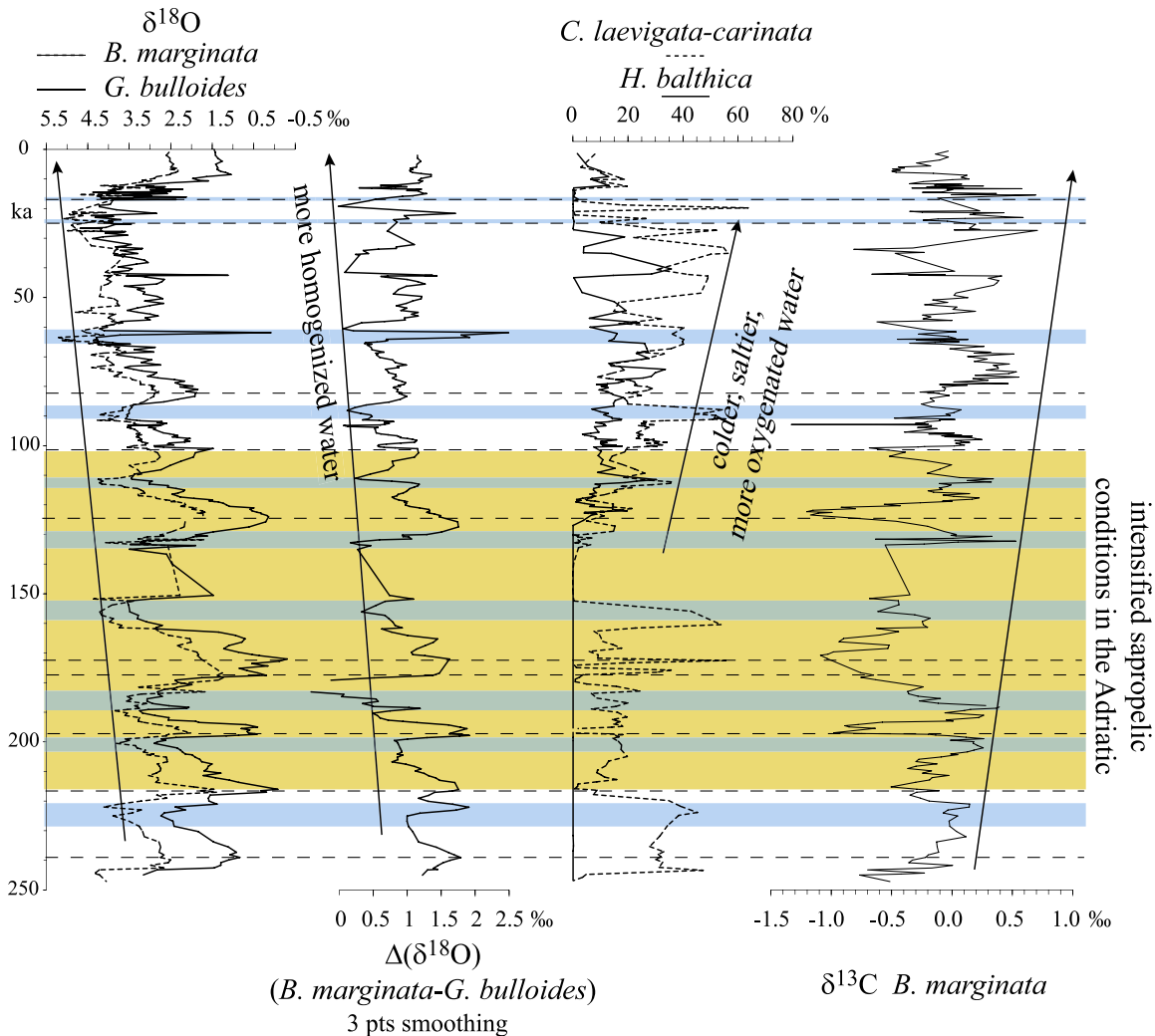
Figure 9. PRAD1-2 integrated proxies (δ^{18}O *G. bulloides* and *B. marginata*, $\Delta(\delta^{18}$O) *B. marginata* – *G. bulloides*, percentages of *H. balthica* and *C. laevigata carinata*, δ^{13}C *B. marginata*) showing the overall trend for the last 250 ka. Blue stripes mark glacial and stadial intervals, while dashed lines define the midpoint of sapropel-equivalent layers. The yellow area indicates the interval when the central Adriatic was more influenced by the monsoon regime.

a 170 m water depth sill located between middle and southern Adriatic (see Figure 1).

6. Conclusions

[46] The analysis of PRAD1-2 multiproxy record provides new evidence for paleoenvironmental trends that appear consistent with those typical for western and eastern Mediterranean basins, apart from some peculiar characteristics like a higher-amplitude temperature excursion during major Terminations (up to 19.5°C during T II) and minor climate transitions, and the deepening trend of glacial intervals from MIS 10 to MIS 4.

[47] Four general conclusions can be drawn from the analysis of the results of PRAD1-2 and their comparison to other paleoceanographic records in the Mediterranean and North Atlantic.

[48] 1. The central Adriatic reflects paleoclimatic changes during the last 370 ka that appear in phase with the North Atlantic climate system except for the interval between MIS 7.5 and MIS 5.3 when the Adriatic basin was more influenced by the monsoon regime.

[49] 2. The Adriatic Basin does not seem capable of maintaining interglacial and interstadial warm conditions over an interval comparable to that reconstructed in the western Mediterranean. The reasons are probably the landlocked position of this shallow basin and the response to other factors such as (1) a greater exposition to atmospheric

forcing, particularly through northerly polar continental air outbreaks, (2) a higher influence of the surrounding landmass, including the occurrence of glaciers on its western side, when the sea level was more than 100 m lower than at present during glacial intervals, resulting in a lag in the demise of glacial conditions, and (3) a higher-latitude position compared to other Mediterranean sites.

[50] 3. During the modern interglacial the Adriatic basin is a site for dense deeper water formation and was so also during past interglacials, contributing to the ventilation of the deep Mediterranean Sea, except when sapropelic conditions became established.

[51] 4. Finally, the analysis of Adriatic cold sapropel, equivalents S4 and S8 clarifies their stratigraphic position: the former is coeval with Alboran AS24 cold oscillation and with ORL6, the latter occurs at the very base of MIS 7.3. Major paleoceanographic turnovers in paleoproductivity seem to have characterized both sapropel-equivalent events, driven by the coupled action of cold climate and enhanced river runoff.

Acknowledgments

References

Alve, E. (1995), Benthic foraminiferal responses to estuarine pollution: A review, *J. Foraminiferal Res.*, *25*(3), 190–203.

Ariztegui, D., et al. (2000), Paleoclimate and the formation of sapropel S1: Inferences from Late Quaternary lacustrine and marine sequences in the central Mediterranean region, *Palaeogeogr. Palaeoclimatol. Palaeoecol.*, *158*, 215–240.

Artegiani, A., D. Bregant, E. Paschini, N. Pinardi, F. Raicich, and A. Russo (1997), The Adriatic Sea general circulation. Part I: Air-sea interactions and water mass structure, *J. Phys. Oceanogr.*, *27*, 1492–1514.

Asioli, A. (1996), High resolution foraminifera biostratigraphy in the central Adriatic basin during the last deglaciation: A contribution to the PALICLAS project, in *Palaeoenvironmental Analysis of Italian Crater Lake and Adriatic Sediments*, *Mem. Ist. Ital. Idrobiol.*, vol. 55, edited by F. Oldfield and P. Guilizzoni, pp. 197–218, Ist. Ital. di Idrobiol., Verbiana-Pallanza, Italy.

Asioli, A., F. Trincardi, J. J. Lowe, and F. Oldfield (1999), Short-term climate changes during the Last Glacial–Holocene transition: Comparison between Mediterranean re-

cords and the GRIP event stratigraphy, *J. Quat. Sci.*, *14*, 373–381.

Asioli, A., F. Trincardi, J. J. Lowe, D. Ariztegui, L. Langone, and F. Oldfield (2001), Sub-millennial scale climatic oscillations in the central Adriatic during the Lateglacial: Palaeoceanographic implications, *Quat. Sci. Rev.*, *20*, 1201–1221.

Bassinot, F. C., L. D. Labeyrie, E. Vincent, X. Quidelleur, N. J. Shackleton, and Y. Lancelot (1994), The astronomical theory of climate and the age of the Brunhes Matuyama magnetic reversal, *Earth Planet. Sci. Lett.*, *126*, 91–108.

Berger, A., and M. F. Loutre (1991), Insolation values for the climate of the last 10 million years, *Quat. Sci. Rev.*, *10*(4), 297–317.

Bourne, A. J. (2006), An initial tephrochronology for the Adriatic core PRAD1-2 for 40 ka BP, M.Sc. thesis, 172 pp., Royal Holloway, Univ. of London, London.

Cacho, I., J. O. Grimalt, M. Canals, L. Sbaffi, N. J. Shackleton, J. Schönfeld, and R. Zahn (2001), Variability of the western Mediterranean Sea surface temperature during the last 25,000 years and its connection with the Northern Hemisphere climatic changes, *Paleoceanography*, *16*, 40–52.

Cacho, I., N. J. Shackleton, H. Elderfield, F. J. Sierro, and J. O. Grimalt (2006), Glacial rapid variability in deep-water temperature and $\delta^{18}O$ from the western Mediterranean Sea, *Quat. Sci. Rev.*, *25*, 3294–3311.

Capotondi, L., M. S. Principato, C. Morigi, F. Sangiorgi, P. Maffioli, S. Giunta, A. Negri, and C. Corselli (2006), Foraminiferal variations and stratigraphic implications to the deposition of sapropel S5 in the eastern Mediterranean, *Palaeogeogr. Palaeoclimatol. Palaeoecol.*, *235*, 48–65.

Casford, J. S. L., E. J. Rohling, R. H. Abu-Zied, C. F. Fontanier, J. Jorissen, M. J. Leng, G. Schmiedl, and J. Thomson (2003), A dynamic concept for eastern Mediterranean circulation and oxygenation during sapropel formation, *Palaeogeogr. Palaeoclimatol. Palaeoecol.*, *190*, 103–119.

Cattaneo, A., and F. Trincardi (1999), The late-Quaternary transgressive record in the Adriatic epicontinental sea: Basin widening and facies partitioning, in *Isolated Shallow Marine Sand Bodies: Sequence Stratigraphic Analysis and Sedimentologic Interpretation*, edited by K. Bergman and J. Snedden, *Spec. Publ. SEPM Soc. Sediment. Geol.*, *64*, 127–146.

Cattaneo, A., B. Dennielou, N. Sultan, A. Asioli, D. Ridente, F. Trincardi, L. Vigliotti, M. Canals, R. Urgeles, and R. Gelfort (2006), EC-PROMESS1 project: Stratigraphic synthesis and geotechnical characterisation of borehole PRAD2 (Lateglacial-Holocene on the western Adriatic shelf), *Geophys. Res. Abstr.*, *8*, 07807.

Chapman, M. R., N. J. Shackleton, M. Zhao, and G. Eglinton (1996), Faunal and alkenone reconstructions of subtropical North Atlantic surface hydrography and paleotemperature over the last 28 kyr, *Paleoceanography*, *11*, 343–357.

Cita, M. B., C. Vergnaud Grazzini, C. Robert, H. Chamley, N. Ciaranfi, and S. D'Onofrio (1977), Paleoclimatic record of a long deep sea core from the eastern Mediterranean, *Quat. Res.*, *8*, 205–235.

Cramp, A., and G. O'Sullivan (1999), Neogene sapropels in the Mediterranean: A review, *Mar. Geol.*, *153*, 11–28.

Dansgaard, W., et al. (1993), Evidence for general instability of past climate from a 250-kyr ice-core record, *Nature*, *364*, 218–220.

Desprat, S., M. F. Sanchez Goñi, J.-L. Turon, J. Duprat, B. Malaize, and J.-P. Peypouquet (2006), Climatic variability of Marine Isotope Stage 7: Direct land-sea-ice correlation from a multiproxy analysis of a north-western Iberian margin deep-sea core, *Quat. Sci. Rev.*, *25*, 1010–1026.

Desprat, S., M. F. Sanchez Goñi, F. Naughton, J.-L. Turon, J. Duprat, B. Malaize, E. Cortijo, and J.-P. Peypouquet (2007), Climatic variability of the last five isotopic interglacials: Direct land-sea-ice correlation from the multiproxy analysis of north-western Iberian margin deep-sea cores, in *The Climate of Past Interglacials, Dev. Quat. Sci.*, vol. 7, edited by F. Sirocko et al., pp. 375–386, Elsevier, Amsterdam.

Emeis, K.-C., H. M. Schulz, U. Struck, T. Sakamoto, H. Doose, H. Erlenkeuser, M. Howell, D. Kroon, and M. Paterne (1998), Stable isotope and alkenone temperature records of sapropels from sites 964 and 967: Constraining the physical environment of sapropel formation in the eastern Mediterranean Sea, edited by A. H. F. Robertson et al., *Proc. Ocean Drill. Program Sci. Results*, 160, 309–331.

Emeis, K.-C., U. Struck, H. M. Schulz, R. Rosenberg, S. Bernasconi, H. Erlenkeuser, T. Sakamoto, and F. Martinez-Ruiz (2000a), Temperature and salinity variations of Mediterranean Sea surface waters over the last 16,000 years from records of planktonic stable oxygen isotopes and alkenone unsaturation ratios, *Palaeogeogr. Palaeoclimatol. Palaeoecol.*, 158, 259–280.

Emeis, K.-C., T. Sakamoto, R. Wehausen, and H. J. Brumsack (2000b), The sapropel record of the eastern Mediterranean Sea: Results of Ocean Drilling Program Leg 160, *Palaeogeogr. Palaeoclimatol. Palaeoecol.*, 158, 371–395.

Emeis, K.-C., et al. (2003), Eastern Mediterranean surface water temperatures and δ^{18}O composition during deposition of sapropels in the late Quaternary, *Paleoceanography*, 18(1), 1005, doi:10.1029/2000PA000617.

EPICA Community Members (2004), Eight glacial cycles from an Antarctic ice core, *Nature*, 429, 623–628.

Fairbanks, R. G., R. A. Mortlock, T.-C. Chiu, L. Cao, A. Kaplan, T. P. Guilderson, T. W. Fairbanks, and A. L. Bloom (2005), Marine radiocarbon calibration curve spanning 0 to 50,000 years B.P. based on paired ^{230}Th/^{234}U/^{238}U and ^{14}C dates on pristine corals, *Quat. Sci. Rev.*, 24, 1781–1796.

Grimalt, J. O., E. Calvo, and C. Pelejero (2001), Sea surface paleotemperature errors in $U_{37}^{K'}$ estimation due to alkenone measurements near the limit of detection, *Paleoceanography*, 16, 226–232.

Hemleben, C., M. Spindler, and O. R. Anderson (Eds.) (1989), *Modern Planktic Foraminifera*, Springer, New York.

Jennings, A. E., N. J. Weiner, G. Helgadottir, and J. T. Andrews (2004), Modern foraminiferal faunas of the southwestern to northern Iceland shelf: Oceanographic and environmental controls, *J. Foraminiferal Res.*, 34(3), 180–207.

Jorissen, F. J. (1988), Benthic foraminifera from the Adriatic Sea: Principles of phenotypic variation, *Utrecht Micropaleontol. Bull.*, 37, 174 pp.

Jorissen, F. J. (1999), Benthic foraminiferal successions across Late Quaternary Mediterranean sapropels, *Mar. Geol.*, 153, 91–101.

Jorissen, F. J., A. Asioli, A. M. Borsetti, L. Capotondi, J. P. De Visser, F. J. Hilgen, E. J. Rohling, K. Van Der Borg, C. Vergnaud-Grazzini, and W. J. Zachariasse (1993), Late Quaternary central Mediterranean biochronology, *Mar. Micropaleontol.*, 21, 169–189.

Knappertsbusch, M. (1993), Geographic distribution of living and Holocene coccolithophores in the Mediterranean Sea, *Mar. Micropaleontol.*, 21, 219–247.

Labeyrie, L., H. Leclaire, C. Waelbroeck, E. Cortijo, J.-C. Duplessy, L. Vidal, M. Elliot, B. Le Coat, and G. Auffret (1999), Temporal variability of the surface and deep waters of the northwest Atlantic Ocean at orbital and millennial scales, in *Mechanisms of Global Climate Change at Millennial Time Scales, Geophys. Monogr. Ser.*, vol. 112, edited by P. U. Clark, R. S. Webb, and L. D. Keigwin, pp. 77–98, AGU, Washington, D. C.

Laj, C., C. Kissel, and A. P. Roberts (2006), Geomagnetic field behavior during the Iceland Basin and Laschamp geomagnetic excursions: A simple transitional field geometry?, *Geochem. Geophys. Geosyst.*, 7, Q03004, doi:10.1029/2005GC001122.

Langereis, C. G., M. J. Dekkers, G. J. De Lange, M. Paterne, and P. J. M. Van Santvoort (1997), Magnetostratigraphy and astronomical calibration of the last 1.1 Myr from an eastern Mediterranean piston core and dating of short events in the Brunhes, *Geophys. J. Int.*, 129, 75–94.

Lascaratos, A., W. Roether, K. Nittis, and B. Klein (1999), Recent changes in deep water formation and spreading in the eastern Mediterranean sea: A review, *Prog. Oceanogr.*, 44, 5–36.

Linke, P., and G. F. Lutze (1993), Microhabitat preferences of benthic foraminifera: A static concept or a dynamic adaptation to optimize food acquisition?, *Mar. Micropaleontol.*, 20, 215–234.

Lisiecki, L. E., and M. E. Raymo (2005), A Pliocene-Pleistocene stack of 57 globally distributed benthic δ^{18}O records, *Paleoceanography*, 20, PA1003, doi:10.1029/2004PA001071.

Lourens, L. J. (2004), Revised tuning of Ocean Drilling Program Site 964 and KC01B (Mediterranean) and implications for the δ^{18}O, tephra, calcareous nannofossil, and geomagnetic reversal chronologies of the past 1.1 Myr, *Paleoceanography*, 19, PA3010, doi:10.1029/2003PA000997.

Martinson, D. G., N. G. Pisias, J. D. Hays, J. Imbrie, T. C. Moore, and N. J. Shackleton (1987), Age dating and the orbital theory of the ice ages: Development of a high-resolution 0 to 300,000-year chronostratigraphy, *Quat. Res.*, 27, 1–29.

Martrat, B., J. O. Grimalt, C. Lopez-Martinez, I. Cacho, F. J. Sierro, J. A. Flores, R. Zahn, M. Canals, J. H. Curtis, and D. A. Hodell (2004), Abrupt temperature changes in the western Mediterranean over the past 250,000 years, *Science*, 306, 1762–1765.

Martrat, B., J. O. Grimalt, N. J. Shackleton, L. de Abreu, M. A. Hutterli, and T. F. Stocker (2007), Four climate cycles of recurring deep and surface water destabilizations on the Iberian Margin, *Science*, 317, 502–507, doi:10.1126/science.1139994.

McManus, J., D. W. Oppo, and J. L. Cullen (1999), A 0.5-million-year record of millennial-scale climate variability in the North Atlantic, *Science*, 283, 971–975.

Meese, D. A., A. J. Gow, R. B. Alley, G. A. Zielinsky, P. M. Grootes, M. Ram, K. C. Taylor, P. A. Mayewski, and J. F. Bolzan (1997), The Greenland Ice Sheet Project 2 depth-age scale: Methods and results, *J. Geophys. Res.*, 102(12), 26,411–26,423.

Meyers, P. A. (2006), Paleoceanographic and paleoclimatic similarities between Mediterranean sapropels and Cretaceous black shales, *Palaeogeogr. Palaeoclimatol. Palaeoecol.*, 235, 305–320.

Miller, A. A. L., D. B. Scott, and F. S. Medioli (1982), *Elphidium excavatum* (Terquem): Ecophenotypic versus subspecific variation, *J. Foraminiferal Res.*, 12(2), 116–144.

Mix, A. C., E. Bard, and R. Schneider (2001), Environmental processes of the ice age: Land, oceans, glaciers (EPILOG), *Quat. Sci. Rev.*, 20, 627–657.

Morigi, C., F. J. Jorissen, S. Fraticelli, B. J. Horton, M. Principi, A. Sabbatini, L. Capotondi, P. V. Curzi, and A. Negri (2005), Benthic foraminiferal evidence for the formation of the Holo-

cene mud-belt and bathymetrical evolution in the central Adriatic Sea, *Mar. Micropaleontol.*, 57, 25–49.

Murray, J. W. (2006), *Ecology and Applications of Benthic Foraminifera*, Cambridge Univ. Press, New York.

Myers, P. G., K. Haines, and E. J. Rohling (1998), Modeling the paleocirculation of the Mediterranean: The last glacial maximum and the Holocene with emphasis on the formation of sapropel S_1, *Paleoceanography*, 13(6), 586–606.

Negri, A., L. Capotondi, and J. Keller (1999), Calcareous nannofossils, planktonic foraminifera and oxygen isotopes in the late Quaternary sapropels of the Ionian Sea, *Mar. Geol.*, 157, 89–103.

Oldfield, F., et al. (2003), A high resolution late Holocene palaeo environmental record from the central Adriatic Sea, *Quat. Sci. Rev.*, 22, 319–342.

Pelejero, C., J. O. Grimalt, S. Heilig, M. Kienast, and L. Wang (1999a), High-resolution $U_{37}^{k'}$ temperature reconstructions in the South China Sea over the past 220 kyr, *Paleoceanography*, 14(2), 224–231.

Pelejero, C., J. O. Grimalt, M. Sarnthein, L. Wang, and J. A. Flores (1999b), Molecular biomarker record of sea surface temperature and climatic change in the South China Sea during the last 140,000 years, *Mar. Geol.*, 156, 109–121.

Perez-Folgado, M., F. J. Sierro, J. A. Flores, J. O. Grimalt, and R. Zahn (2004), Paleoclimatic variations in foraminifer assemblages from the Alboran Sea (western Mediterranean) during the last 150 ka in ODP Site 977, *Mar. Geol.*, 212, 113–131.

Petit, J. R., et al. (1999), Climate and atmospheric history of the past 420,000 years from the Vostok ice core, Antarctica, *Nature*, 399, 429–436.

Pierre, C., P. Belanger, J. F. Saliege, M. J. Urrutiaguer, and A. Murat (1999), Paleoceanography of the western Mediterranean during the Pleistocene: Oxygen and carbon isotope records at Site 975, *Proc. Ocean Drill. Program Sci. Results*, 161, 481–488.

Piva, A., A. Asioli, R. R. Schneider, F. Trincardi, N. Andersen, E. Colmenero-Hidalgo, B. Dennielou, J.-A. Flores, and L. Vigliotti (2008), Climatic cycles as expressed in sediments of the PROMESS1 borehole PRAD1-2, central Adriatic, for the last 370 ka: 1. Integrated stratigraphy, *Geochem. Geophys. Geosyst.*, 9, Q01R01, doi:10.1029/2007GC001713.

Prahl, F. G., and S. G. Wakeham (1987), Calibration of unsaturation patterns in long-chain ketone compositions for paleotemperature assessment, *Nature*, 330, 367–369.

Pujol, C., and C. Vergnaud Grazzini (1995), Distribution patterns of live planktic foraminifera as related to regional hydrography and productive systems of the Mediterranean Sea, *Mar. Micropaleontol.*, 25, 187–217.

Rio, D., I. Raffi, and G. Villa (1990), Pliocene-Pleistocene calcareous nannofossil distribution patterns in the western Mediterranean, *Proc. Ocean Drill. Program Sci. Results*, 107, 513–533.

Rodrigues, C. G., and K. Hopper (1982), The ecological significance of *Elphidium clavatum* in the Gulf of St. Lawrence, Canada, *J. Paleontol.*, 56(2), 410–422.

Rohling, E. J. (1994), Review and new aspects concerning the formation of eastern Mediterranean sapropels, *Mar. Geol.*, 122, 1–28.

Rohling, E. J., F. J. Jorissen, C. Vergnaud-Grazzini, and W. J. Zachariasse (1993), Northern Levantine and Adriatic Quaternary planktic foraminifera: Reconstruction of paleonvironmental gradients, *Mar. Micropaleontol.*, 21(1), 191–218.

Rohling, E. J., F. J. Jorissen, and H. C. De Stigter (1997), 200-year interruption of Holocene sapropel formation in the Adriatic Sea, *J. Micropaleontol.*, 16, 97–108.

Rohling, E. J., P. A. Mayewski, R. H. Abu-Zied, J. S. L. Casford, and A. Hayes (2002), Holocene atmosphere-ocean interactions: Records from Greenland and the Aegean Sea, *Clim. Dyn.*, 18, 587–593.

Rossignol-Strick, M. (1983), African monsoons, an immediate response to orbital insolation, *Nature*, 304, 46–49.

Rossignol-Strick, M., W. Nesteroff, P. Olive, and C. Vergnaud-Grazzini (1982), After the deluge: Mediterranean stagnation and sapropel formation, *Nature*, 295, 105–110.

Roucroux, K. H., P. C. Tzedakis, L. de Abreu, and N. J. Shackleton (2007), Fine-tuning the land ocean correlation for the late middle Pleistocene of southern Europe, in *The Climate of Past Interglacials*, *Dev. Quat. Sci.*, vol. 7, edited by F. Sirocko et al., pp. 359–373, Elsevier, Amsterdam.

Sangiorgi, F., L. Capotondi, N. Combourieu Nebout, L. Vigliotti, H. Brinkhuis, S. Giunta, A. F. Lotter, C. Morigi, A. Negri, and G.-J. Reichart (2003), Holocene seasonal sea-surface temperature variations in the southern Adriatic Sea inferred from a multiproxy approach, *J. Quat. Sci.*, 18(8), 723–732.

Sanvoisin, R., S. D'Onofrio, R. Lucchi, D. Violanti, and D. Castradori (1993), 1 Ma paleoclimatic record from the eastern Mediterranean-Marflux project: First results of a micropaleontological and sedimentological investigation of a long piston core from the Calabrian Ridge, *Quaternario*, 6(2), 169–188.

Schmiedl, G., C. Hemleben, J. Keller, and M. Segl (1998), Impact of climatic changes on the benthic foraminiferal fauna in the Ionian Sea during the last 330,000 years, *Paleoceanography*, 13(5), 447–458.

Shackleton, N. J. (2000), The 100,000-Year Ice-Age cycle identified and found to lag temperature, carbon dioxide, and orbital eccentricity, *Science*, 289, 1897–1902.

Stuiver, M., and P. J. Reimer (1993), Extended ^{14}C data base and revised CALIB 3.0 ^{14}C age calibration program, *Radiocarbon*, 35, 215–230.

Totti, C., G. Civitarese, F. Acri, D. Barletta, G. Candelari, E. Paschini, and A. Solazzi (2000), Seasonal variability of phytoplankton populations in the middle Adriatic sub-basin, *J. Plankton Res.*, 22(9), 1735–1756.

Trincardi, F., A. Correggiari, and M. Roveri (1994), Late-Quaternary transgressive erosion and deposition in a modern epicontinental shelf the Adriatic semienclosed basin, *Geo Mar. Lett.*, 14, 41–51.

Tzedakis, P. C., K. H. Roucoux, L. de Abreu, and N. J. Shackleton (2004), The duration of forest stages in southern Europe and interglacial climate variability, *Science*, 306, 2231–2235.

Van der Zwaan, G. J., and F. J. Jorissen (1991), Biofacial pattern in river induced shelf anoxia, in *Modern and Ancient Continental Shelf Anoxia*, edited by R. V. Tyson and T. H. Pearson, *Geol. Soc. Spec. Publ.*, 58, 65–82.

Vergnaud-Grazzini, C., W. B. F. Ryan, and M. B. Cita (1977), Stable isotope fractionation, climate change and episodic stagnation in the eastern Mediterranean during the Late Quaternary, *Mar. Micropaleontol.*, 2, 353–370.

Vilks, G. (1989), Ecology of recent foraminifera on the Canadian continental shelf of the Arctic Ocean, in *The Arctic Seas, Climatology, Oceanography, Geology, and Biology*, edited by Y. Herman, pp. 497–569, Van Nostrand Reinhold, New York.

Villanueva, J., C. Pelejero, and J. O. Grimalt (1997), Clean-up procedures for the unbiased estimation of C_{37} alkenones sea

surface temperatures and terrigenous n-alkane inputs in paleoceanography, *J. Chromatogr.*, *757*, 145–151.

Villanueva, J., J.-A. Flores, and J. O. Grimalt (2002), A detailed comparison of the Uk′$_{37}$ and coccolith records over the past 290 kyears: Implications to the alkenone paleotemperature method, *Org. Geochem.*, *33*, 897–905.

Weldeab, S., R. R. Schneider, and P. Müller (2007), Comparison of Mg/Ca- and alkenone-based sea surface temperature estimates in the fresh water–influenced Gulf of Guinea, eastern equatorial Atlantic, *Geochem. Geophys. Geosyst.*, *8*, Q05P22, doi:10.1029/2006GC001360.

Wilkinson, I. P. (1979), The taxonomy, morphology and distribution of the Quaternary and recent foraminifer *Elphidium clavatum* Cushman, *J. Paleontol.*, *53*(3), 628–641.

Williamson, M. A., C. E. Keen, and P. J. Mudie (1984), Foraminiferal distribution on the continental margin off Nova Scotia, *Mar. Micropaleontol.*, *9*, 219–239.

Wulf, S., M. Kraml, A. Brauer, J. Keller, and J. F. W. Negendank (2004), Tephrochronology of the 100 ka lacustrine sediment record of Lago Grande di Monticchio (southern Italy), *Quat. Int.*, *122*, 7–30.